

COURSE OBJECTIVES

1. To provide an overview of factors affecting the behavior of materials in components.
2. To expose students to understand the mechanism of fracture.
3. To Study and acquire knowledge on Dynamic and Time-dependent fracture.
4. To study the features of fracture toughness values.
5. To provide an overview of life prediction
6. To Study and acquire knowledge on failure analysis tools in industries

UNIT I MATERIALS AND DESIGN PROCESS**9**

Factors affecting the behavior of materials in components, effect of component geometry and shape factors, design for static strength, stiffness, designing with high strength and low toughness materials, designing for hostile environments, material processing and design, processes and their influence on design, process attributes, systematic process selection, screening, process selection diagrams, ranking, process cost.

UNIT II FRACTURE MECHANICS**9**

Ductile fracture, brittle fracture, Cleavage-fractography, ductile-brittle transition-Fracture mechanics approach to design-energy criterion, stress intensity approach, time dependent crack growth and damage. Linear Elastic Fracture Mechanics - Griffith theory, Energy release rate, instability and R-curve, stress analysis of cracks- stress intensity factor, K-threshold, crack growth instability analysis, crack tip stress analysis. Elastic Plastic Fracture Mechanics - Crack tip opening displacement(CTOD), J integral, relationship between J and CTOD,

UNIT III DYNAMIC AND TIME-DEPENDENT FRACTURE**9**

Dynamic fracture, rapid loading of a stationary crack, rapid crack propagation, dynamic contour integral, Creep crack growth-C Integral, Visco elastic fracture mechanics, viscoelastic J integral

UNIT IV DETERMINATION OF FRACTURE TOUGHNESS VALUES**9**

Experimental determination of plane strain fracture toughness, K- R curve testing, J measurement, CTOD testing, effect of temperature, strain rate on fracture toughness.

UNIT V FAILURE ANALYSIS TOOLS**9**

Reliability concept and hazard function, life prediction, life extension, application of poisson, exponential and Weibull distribution for reliability, bath tub curve, parallel and series system, MTBF,MTTR, FMEA definition- Design FMEA, Process FMEA , analysis causes of failure, modes, ranks of failure modes, fault tree analysis, industrial case studies/projects on FMEA.

Text Books

S. No.	Author(s) Name	Title of the book	Publisher	Year of Publication
1	John M Barsoom and Stanley T Rolte	Fracture and Fatigue Control in Structures	Prentice Hall, New Delhi	1987
2	Michael F Ashby	Material Selection in Mechanical Design	Butterworth – Heinemann	2005

References

S. No.	Author(s) Name	Title of the book	Publisher	Year of Publication
1	Shigley and Mische	Mechanical Engineering Design	McGraw Hill Inc., New York	1992
2	Mahmoud M Farag	Material Selection for Engineering Design	Prentice Hall, New Delhi	1997
3	Faculty of Mechanical Engineering	Design Data Book	PSG College of Technology, DPV Printers, Coimbatore	1993
4	ASM Metals Handbook	Failure Analysis and Prevention	ASM Metals Park, Ohio, USA,	1995



KARPAGAM ACADEMY OF HIGHER EDUCATION

(Deemed to be University Established Under Section 3 of UGC Act, 1956)

Eachanari Post, Coimbatore-641021, INDIA

FACULTY OF ENGINEERING

DEPARTMENT OF MECHANICAL ENGINEERING (AUTOMOBILE)

LESSON PLAN

Subject Name : Failure Analysis and Design
Subject Code : 15BEME6E04
Name of the Faculty : Mr. A. J. R. Nelson
Designation : Assistant Professor
Year / Semester : III / VI
Branch : Mechanical Engineering

Sl. No.	No. of Periods	Topics to be Covered	Support Materials
<u>UNIT-I: MATERIALS AND DESIGN PROCESS</u>			
1.	1	Factors affecting the behavior of materials in components	T1, R1
2.	1	effect of component geometry and shape factors	T1, R1
3.	1	design for static strength, stiffness	T1, R1
4.	1	designing with high strength and low toughness materials	T1, R1
5.	1	designing for hostile environments, material processing and design	T1, R1
6.	1	processes and their influence on design	T1, R1
7.	1	process attributes, systematic process selection	T1, R1
8.	1	screening, process selection diagrams,	T1, R1
9.	1	ranking, process cost	T1, R1
Total no. of hours planned for Unit-I			09

Sl. No.	No. of Periods	Topics to be Covered	Support Materials
<u>UNIT-II: FRACTURE MECHANICS</u>			
10.	1	Ductile fracture, brittle fracture, Cleavage-fractography	T2, R2
11.	1	ductile-brittle transition-Fracture mechanics approach to design	T2, R2
12.	1	energy criterion, stress intensity approach, time dependent crack growth and damage	T2, R2

STRENGTH OF MATERIALS LESSON PLAN

13.	1	Linear Elastic Fracture Mechanics	T2, R2
14.	1	Griffith theory, Energy release rate, instability and R-curve	T2, R2
15.	1	stress analysis of cracks- stress intensity factor, K-threshold	T2, R2
16.	1	crack growth instability analysis	T2, R2
17.	1	crack tip stress analysis. Elastic Plastic Fracture Mechanics	T2, R2
18.	1	Crack tip opening displacement (CTOD), J integral, relationship between J and CTOD	T2, R2
Total no. of hours planned for Unit-II			09

Sl. No.	No. of Periods	Topics to be Covered	Support Materials
<u>UNIT-III: DYNAMIC AND TIME-DEPENDENT FRACTURE</u>			
19.	1	Dynamic fracture	T3, R3
20.	1	rapid loading of a stationary crack	T3, R3
21.	1	rapid crack propagation	T3, R3
22.	1	dynamic contour integral	T3, R3
23.	1	Creep crack growth	T3, R3
24.	1	C Integral	T3, R3
25.	1	Visco elastic fracture mechanics	T3, R3
26.	1	viscoelastic J integral	T3, R3
27.	1	Visco Elastic FM and J – Integral Flash	T3, R3
Total no. of hours planned for Unit-III			09

Sl. No.	No. of Periods	Topics to be Covered	Support Materials
<u>UNIT-IV: DETERMINATION OF FRACTURE TOUGHNESS VALUES</u>			
28.	1	Experimental determination of plane strain fracture toughness	T3, R3
29.	1	K Curve	T3, R3
30.	1	R Curve	T3, R3
31.	1	K- R curve testing	T3, R3
32.	1	J measurement	T3, R3
33.	1	CTOD testing	T3, R3
34.	1	effect of temperature	T3, R3
35.	1	strain rate	T3, R3

STRENGTH OF MATERIALS LESSON PLAN

36.	1	strain rate on fracture toughness	T3, R3
Total no. of hours planned for Unit-III			09

Sl. No.	No. of Periods	Topics to be Covered	Support Materials
<u>UNIT-V: FAILURE ANALYSIS TOOLS</u>			
37.	1	Reliability concept and hazard function	T3, R4
38.	1	life prediction, life extension	T3, R4
39.	1	application of poisson	T3, R4
40.	1	exponential and Weibull distribution for reliability	T3, R4
41.	1	bath tub curve	T3, R4
42.	1	parallel and series system, MTBF,MTTR, FMEA definition	T3, R4
43.	1	Design FMEA, Process FMEA	T3, R4
44.	1	analysis causes of failure, modes, ranks of failure modes	T3, R4
45.	1	fault tree analysis, industrial case studies/projects on FMEA.	T3, R4
Total no. of hours planned for Unit-V			09

TOTAL PERIODS : 45

TEXT BOOKS:

SL. NO.	AUTHOR(S)	TITLE OF THE BOOK	PUBLISHER	YEAR OF PUBLICATION
1.	John M Barsoom and Stanley T Rolte	Fracture and Fatigue Control in Structures	Prentice Hall, New Delhi	1987
2.	Michael F Ashby	Material Selection in Mechanical Design	Butterworth – Heinemann	2005
3.	Shigley and Mische	Mechanical Engineering Design	McGraw Hill Inc., New York	1992

REFERENCE BOOKS:

SL. NO.	AUTHOR(S)	TITLE OF THE BOOK	PUBLISHER	YEAR OF PUBLICATION
1.	Mahmoud M Farag	Material Selection for Engineering Design	Prentice Hall, New Delhi	1997
2.	Faculty of Mechanical Engineering	Design Data Book	PSG College of Technology, DPV	1993

STRENGTH OF MATERIALS LESSON PLAN

			Printers, Coimbatore	
3.	ASM Metals Handbook	Failure Analysis and Prevention	ASM Metals Park, Ohio, USA,	1995
4.	Charles Brooks	Failure Analysis of Engineering Materials	Tata Mcgraw-Hill	2002

UNIT	Total No. of Periods Planned	Lecture Periods
I	09	09
II	09	09
III	09	09
IV	09	09
V	09	09
TOTAL	45	45

I.	CONTINUOUS INTERNAL ASSESSMENT (Internal Assessment Tests: 30, Attendance: 5, Seminar: 5)	: 40 Marks
II.	END SEMESTER EXAMINATION	: 60 Marks
	TOTAL	: 100 Marks

FACULTY

HOD / MECHANICAL

DEAN / FOE

UNIT I - MATERIALS AND DESIGN PROCESS

Factors Affecting Fatigue Performance

Many parameters affect the fatigue performance of structural components. They include parameters related to stress (load), geometry and properties of the component, and the external environment. The stress parameters include state of stress, stress range, stress ratio, constant or variable loading, frequency, and maximum stress. The geometry and properties of the component include stress

(strain) raisers, size, stress gradient, and metallurgical and mechanical properties of the base metal and weldments. The external environment parameters include temperature and aggressiveness of the environment. The effects of most of these parameters are discussed in the following chapters. The primary factor that affects the fatigue behavior of structural components is the fluctuation in the localized stress or strain. Consequently, the most effective methods for increasing the fatigue life significantly are usually accomplished by decreasing the severity of the stress concentration and the magnitude of the applied nominal stress. In many cases, a decrease in the severity of the stress concentration can be easily accomplished by using transition radii in fillet regions, keyways, geometrical changes, and by minimizing the size of weld discontinuities. The corrosion-fatigue behavior of components is affected by the same parameters that affect the fatigue behavior as well as factors that do not affect fatigue, for example, frequency and waveform of the stress cycle and the environment. Unfortunately, at present, the only means of determining the corrosion-fatigue behavior of materials is by conducting the tests on the actual material-environment system of interest.

Shape Factors

Shaped sections carry bending, torsional and axial-compressive loads more efficiently than solid sections do. By 'shaped' we mean that the cross-section is formed to a tube, a box-section, an I-section or the like. By 'efficient' we mean that, for given loading conditions, the section uses as little material, and is therefore as light, as possible. Tubes, boxes and I-sections will be referred to as 'simple shapes'. Even greater efficiencies are possible with sandwich panels (thin load-bearing skins bonded to a foam or honeycomb interior) and with structures (the Warren truss, for instance). This chapter extends the concept of indices so as to include shape (Figure 7.1). Often it is not necessary to do so: in the case studies of Chapter 6, shape either did not enter at all, or, when it did, it was not a variable (that is, we compared materials with the same shape). But when two materials are available with different section shapes and the design is one in which shape matters (a beam in bending, for example), the more

general problem arises: how to choose, from among the vast range of materials and the section shapes in which they are available -or could, potentially, be made -the one which maximizes the performance. Take the example of a bicycle: its forks are loaded in bending. It could, say, be made of steel or of wood -early bikes were made of wood. But steel is available as thin-walled tube, whereas the wood is not; wood, usually, has a solid section. A solid wood bicycle is certainly lighter and stiffer than a solid steel one, but is it better than one made of steel tubing? Might a magnesium I-section be better still? What about a webbed polymer moulding? How, in short, is one to choose the best combination of material and shape? A procedure for answering these and related questions is outlined in this chapter. It involves the definition of shape factors: simple numbers which characterize the efficiency of shaped sections. These allow the definition of material indices which are closely related to those of Chapter 5, but which now include shape. When shape is constant, the indices reduce exactly to those of Chapter 5; but when shape is a variable, the shape factor appears in the expressions for the indices. The ideas in this chapter are a little more difficult than those of Chapter 5; their importance lies in the connection they make between materials selection and the designs of load-bearing structures. A feel for the method can be had by reading the following section and the final section alone; these, plus the results listed in Tables 7.1 and 7.2, should be enough to allow the case studies of Chapter 8 (which apply the method) to be understood. The reader who wishes to grasp how the results arise will have to read the whole thing. There are practical limits for the thinness of sections, and these determine, for a given material, the maximum attainable efficiency. These limits may be imposed by manufacturing constraints: the difficulty or expense of making an efficient shape may simply be too great. More often they are imposed by the properties of the material itself because these determine the failure mode of the section. Here we explore the ultimate limits for shape efficiency. This we do in two ways. The first (this section) is empirical: by examining the shapes in which real materials - steel, aluminium, etc. - are actually made, recording the limiting efficiency of available sections. The second is by the analysis of the mechanical stability of shaped sections, explored in the following section. Standard sections for beams, shafts, and columns are generally prismatic; prismatic shapes are easily made by rolling, extrusion, drawing, pultrusion or sawing. Figure 7.5 shows the taxonomy of the kingdom of prismatic shapes. The section may be solid, closed-hollow (like a tube or box) or open-hollow (an I-, U- or L-section, for instance). Each class of shape can be made in a range of materials. Those for which standard, off-the-shelf, sections are available are listed on the figure: steel, aluminium, GFRP and wood. Each section has a set of attributes: they are the parameters used in structural or mechanical design. They include its dimensions and its section properties (the 'moments' I , K and the 'section moduli' Z and Q) defined in the previous section.

These are what we need to allow the limits of shape to be explored. Figures 7.6 show I, K, Z and Q plotted against A, on logarithmic scales for standard steel sections. Consider the first, Figure 7.6(a). It shows $\log(I)$ plotted against $\log(A)$.

Designing for simple axial loading

When the component is subjected to uniaxial stress, yielding will take place when the local stress reaches the yield strength of the material. The critical cross-sectional area, A, of such component can be estimated as:

$$A = KtnL / YS$$

Where

Kt = stress concentration factor

L = applied load

n = factor of safety

YS = yield strength of the material

Designing for torsional loading

The critical cross-sectional area of a circular shaft subjected to torsional loading can be determined from the relationship:

Designing for bending

When a relatively long beam is subjected to bending, the bending moment, the maximum allowable stress, and dimensions of the cross section are related by the equation:

$$Z = (nM)/YS$$

where M = bending moment.

Z = section modulus = I/c.

I = moment of inertia of the cross section with respect to the neutral axis normal to the direction of the load.

c = distance from center of gravity of the cross section to the outermost fiber.

Introduction and synopsis

‘Design’ is one of those words that means all things to all people. Every manufactured thing, from the most lyrical of ladies’ hats to the greasiest of gearboxes, qualifies, in some sense or other, as a design. It can mean yet more. Nature, to some is Divine Design; to others it is design by Natural Selection, the ultimate genetic algorithm. The reader will agree that it is necessary to narrow the field, at least a little.

This book is about mechanical design, and the role of materials in it. Mechanical components have mass; they carry loads; they conduct heat and electricity; they are exposed to wear and to corrosive environments; they are made of one or more materials; they have shape; and they must be manufactured (Figure 1.1). The book describes how these activities are related. Materials have limited design since man first made clothes, built shelters and waged wars. They still do. But materials and processes to shape them are developing faster now than at any previous time in history; the challenges and opportunities they present are greater than ever before. The book develops a strategy for exploiting materials in design.

Materials in design

Design is the process of translating a new idea or a market need into the detailed information from which a product can be manufactured. Each of its stages requires decisions about the materials from which the product is to be made and the process for making it. Normally, the choice of material is dictated by the design. But sometimes it is the other way round: the new product, or the evolution of the existing one, was suggested or made possible by the new material. The number of materials available to the engineer is vast: something between 40 000 and 80 000 are at his or her (from here on 'his' means both) disposal. And although standardization strives to reduce the number, the continuing appearance of new materials with novel, exploitable, properties expands the options further. How, then, does the engineer choose, from this vast menu, the material best suited to his purpose? Must he rely on experience? Or can a systematic procedure be formulated for making a rational choice? The question has to be answered at a number of levels, corresponding to the stage the design has reached. At the beginning the design is fluid and the options are wide; all materials must be considered. As the design becomes more focused and takes shape, the selection criteria sharpen and the shortlist of materials which can satisfy them narrows. Then more accurate data are required (although for a lesser number of materials) and a different way of analysing the choice must be used. In the final stages of design, precise data are needed, but for still fewer materials – perhaps only one. The procedure must recognize the initial richness of choice, narrow this to a small subset, and provide the precision and detail on which final design calculations can be based.

Selecting the optimum combination of material and process cannot be performed at one certain stage in the history of a project, it should gradually evolve during the different stages of product development. After identifying the function of the component, the following questions become important:

- What are the primary design and material requirements?

- What are the secondary requirements and are they necessary?

General steps in materials selection

1. Analysis of the performance requirements.
2. Development of alternative solutions to the problem.
3. Evaluation of the different solutions.
4. Decision on the optimum solution.

Creating alternative solutions

Having specified the material requirements, the rest of the selection process involves the search for the material that would best meet those requirements. The starting point is the entire range of engineering materials. At this stage, it is essential to open up channels in different directions. A steel may be the best material for one design concept while a plastic is best for a different concept, even though the two designs provide similar functions.

Initial screening of solutions I

Rigid materials and process requirements. Initial screening of materials can be achieved by first classifying their performance requirements into two main categories:

- Rigid, or go-no-go, requirements.
- Soft, or relative, requirements.

Materials that do not satisfy the rigid requirements are eliminated. For example, metals and alloys are eliminated when selecting materials for an electrical insulator.

Selecting the optimum material for a cryogenic storage tank

Materials requirements:

- used in cryogenic applications for liquefied nitrogen gas) must not suffer ductile-brittle transition at -196°C
- Using stronger material gives thinner walls, which means a lighter tank, lower cool down losses, and easier to weld.
- Lower specific gravity gives lighter tank.
- Lower specific heat reduces cool down losses.
- Lower thermal expansion coefficient reduces thermal stress.
- Lower thermal conductivity reduces heat losses.
- The cost of material and processing will be used as a modifier to the material performance index.

UNIT II – FRACTURE MECHANICS

Ductile Fracture

A ductile fracture is a type of fracture characterized by extensive plastic deformation or necking. This usually occurs prior to the actual fracture. In a ductile fracture, there is absorption of massive amounts of energy and a slower propagation before the fracture occurs as compared to a brittle fracture. All fracture processes involve two steps, crack formation and propagation, which are responses to imposed stress. The rate of the fracture is highly dependent on the mechanics of the crack propagation. Cracks that occur in ductile materials are said to be stable, meaning they are able to resist extension without any increase in stress. However, in brittle materials, cracks are unstable, which means that the crack propagation, once started, continues spontaneously without an increase in stress level. By understanding ductile fractures, engineers are able to develop more dependable and safer industrial products and materials. For example, ductility is a desirable property in high temperature and high-pressure applications in reactor plants due to the added stresses on the metals. High ductility in these applications helps to greatly reduce the possibility of a sudden brittle fracture.

Brittle Fracture

Brittle Fracture is the sudden, very rapid cracking of equipment under stress where the material exhibited little or no evidence of ductility or plastic degradation before the fracture occurs. Unlike most other tensile failures, where the material plastically strains under overload conditions and becomes thinner until the point of rupture, when a piece of equipment suffers a brittle fracture, there is no thinning or necking down. Rather, this damage mechanism often causes cracking without warning, sometimes fracturing equipment into many pieces. Brittle fracture is often caused by low temperatures. If the steel temperature is at or below its brittle-to-ductile transition temperature, then it will be susceptible to brittle fracture. Combine this with a critical sized flaw and high stress on that flaw (either applied or residual), and then you are likely to experience a brittle fracture.

Cleavage Fractography

Cleavage is the mechanism of brittle trans granular fracture and occurs through cleaving of the crystals along crystallographic planes. The cleavage planes can be identified by x-ray crystallography and, sometimes through the geometric shape of etch pits. Cleavage facets are best defined in relatively large grained structures, fractured at low temperatures. Fine grain sizes and higher temperatures can lead to the occurrence of quasi-cleavage, which blends cleavage facets with areas of dimple (MVC)

rupture, such that the cleavage steps become tear ridges. The appearance of typical cleavage facets is shown in Figure 1. So-called 'river patterns' are formed when the cleavage fracture is forced to re-initiate at the boundary of a grain in a different orientation (via a step-wise process). These tear ridges tend to merge in the direction of crack growth, and can be used to identify local crack initiation and growth events.

Ductile Brittle Transition

At low temperatures some metals that would be ductile at room temperature become brittle. This is known as a ductile to brittle transition. The ductile to brittle transition temperature is strongly dependant on the composition of the metal. Steel is the most commonly used metal that shows this behaviour. For some steels the transition temperature can be around 0°C, and in winter the temperature in some parts of the world can be below this. As a result, some steel structures are very likely to fail in winter.

Example of Brittle Failure

Ductile fracture is always a preferred mechanism of failure. Many cases have occurred through history where catastrophic failures have occurred as a result of brittle fracture. The most infamous of these is the sinking of the Titanic. The sinking of the titanic was caused primarily by the brittleness of the steel used to construct the hull of the ship. In the icy water of the Atlantic, the steel was below the ductile to brittle transition temperature. In these conditions even a small impact could have caused a large amount of damage. The impact of an iceberg on the ship's hull resulted in brittle fracture of the bolts that were holding the steel plates together. Nowadays engineers know more about this phenomenon and the composition of the steels used is much more controlled, resulting in a lower temperature at which the ductile to brittle transition occurs.

Stress Intensity Factors

The stress intensity factor was developed in 1957 by George R Irwin, the man usually considered to be the father of fracture mechanics [1]. The stress intensity factor is abbreviated SIF and represented by the variable, K . It is one of the most fundamental and useful parameters in all of fracture mechanics. The stress intensity factor describes the stress state at a crack tip, is related to the rate of crack growth, and is used to establish failure criteria due to fracture. Irwin arrived at the definition of K as a near-crack-tip approximation to Westergaard's complete solution for the stress field surrounding a crack [2]. Recall that Westergaard used complex numbers and Airy stress functions to

do so. We will first review Westergaard's solution, and then see how Irwin used it to develop the stress intensity factor.

In most cases, time-dependent crack growth, also referred to as sustained load crack growth, environmentally enhanced crack growth, or creep crack growth, can be characterized on the basis of the stress intensity factor, K , when the crack-tip damage, creep, or plastic zone is small and constrained within the elastic stress field. For K -controlled crack growth, Ni-base alloys typically exhibit a large-crack growth threshold, K_{th} , below which time-dependent crack growth does not occur. The magnitude of the K_{th} is usually higher than the large-crack fatigue crack threshold, ΔK_{th} . Neither the origin nor the magnitude of the time-dependent crack growth threshold, K_{th} , is well understood for oxidation, stress corrosion, or creep crack growth. On the other hand, the crack growth rates during dwell fatigue at elevated temperature in air are significantly higher than the crack growth rates under pure fatigue in air at the same temperature and stress intensity range, ΔK , levels. Ni-base superalloys in advanced turbo-propulsion systems operate at severe temperature and environments where competing cycle-dependent and time-dependent crack growth mechanisms may be operative concurrently. Thus, there is a need for a better understanding of the interactions between cycle-dependent and time-dependent crack growth at the respective near-threshold regimes.

Stress Intensity Factor, K

Note that the numerators of all three stress equations contain the same expression, $\sigma_\infty = \sqrt{\pi a}$. This combination of σ_∞ and a completely describes the severity of the stress state at the crack tip. Irwin recognized this and first used the term stress intensity factor to describe the expression. (Although he didn't include π in the beginning. It was added later.)

$$K = \sigma_\infty \sqrt{\pi a}$$

Linear elastic fracture mechanics (LEFM)

Linear elastic fracture mechanics (LEFM) is based on the analysis of cracks in linear elastic materials. It provides a tool for solving most practical problems in engineering mechanics, such as safety and life expectancy estimation of cracked structures and components.

Griffith theory

The Griffith theory states that a crack will propagate when the reduction in potential energy that occurs due to crack growth is greater than or equal to the increase in surface energy due to the

creation of new free surfaces. This theory is applicable to elastic materials that fracture in a brittle fashion.

Scientific Fundamentals

Through a series of experiments, stress analyses, and synthesis of prior work, in his remarkable paper Griffith (1921) developed the fundamental concept that underlies the modern theory of linear elastic fracture mechanics. His theory is based on balancing the reduction of potential energy that occurs during fracture with the increase in surface energy due to the creation of new free surfaces when a crack grows. The energy release rate, G , is defined as the energy that flows to the crack tip per unit of new crack surface created.

Griffith Theory of Brittle Fracture

Griffith attributed the discrepancy between the observed fracture strength of crystals and the theoretical cohesive strength to the presences of flaws in brittle materials. This theory is applicable only to perfectly brittle material such as glass, and cannot be used directly to metals. However, Griffith's ideas formed a base to understand the fracture in metals.

Griffith proposed that a brittle material contains a large number of fine cracks. He postulated a criterion for the propagation of such a crack in a brittle material. During propagation, there is a release of what is called the elastic strain energy, some of the energy that is stored in the material as it is elastically deformed.

Further-more, during crack propagation, new free surfaces are created as the faces of a crack. This requires energy to overcome the cohesive force of the atoms, that is, it requires an increase in surface energy. Griffith developed a criterion for crack propagation by performing an energy balance using these two energies as- a crack propagates when the decrease in elastic strain energy is atleast equal to the energy required to create the new crack surface. The thermodynamic relationship between these two energies determines the magnitude of the tensile stress needed to propagate a crack of a certain size to produce a brittle fracture. Consider a wide sheet of unit thickness of a brittle material. It has a lens-shaped crack of $2c$ length which runs from the front to the back face as illustrated in Fig. 15.12. When a longitudinal tensile stress, σ is applied, the crack tends to increase its length in the transverse direction (i.e., in a perpendicular direction to the tensile stress).

When the crack spreads, the surface area of the crack increases, but the elastic strain energy stored in the thin sheet decreases because the elastic strains are not continuous across the cracked region. The elastic strain energy released per unit of plate thickness is given by-

$$U_E = -\frac{\pi c^2 \sigma^2}{E} \quad \dots(15.14)$$

where, E is Young's modulus. The negative sign indicates the release of elastic strain energy as the crack grows. As the crack propagates, two surfaces are created. If γ is the surface energy per unit area of the material and as $2c$ is the crack length, the surface energy of the crack is $U_s = 4c\gamma$

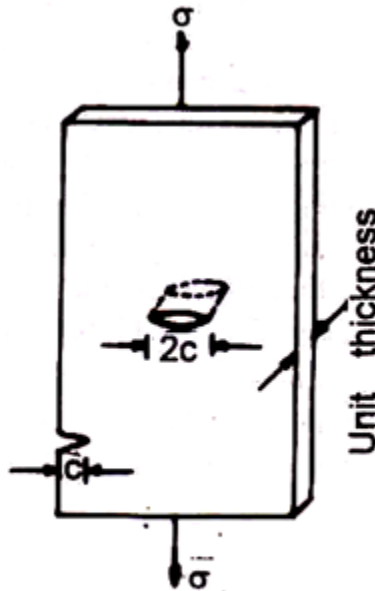


Fig. 15.12. Griffith elliptical crack model.

Now, it is possible to write an energy equation as the crack forms. The change in energy, ΔU as the crack propagates is given by-

$$\Delta U = 4\gamma c - \frac{\pi c^2 \sigma^2}{E} \quad \dots(15.16)$$

Griffith postulated that the crack propagates under a constant applied stress, σ , if an incremental increase in crack length produces no change in the total energy of the system, that is, the Griffith condition for fracture is obtained if the rate at which strain energy is released balances the rate at which energy is required to create the new surfaces, i.e., the critical value is obtained by setting-

$$\frac{d\Delta U}{dc} = 0$$

or

$$\frac{d\Delta U}{dc} = 0 = \frac{d}{dc} \left(4\pi c - \frac{\pi c^2 \sigma^2}{E} \right)$$

$$4\gamma - \frac{2\pi c \sigma^2}{E} = 0$$

$$\sigma_c = \left(\frac{2E\gamma}{\pi c} \right)^{1/2} \quad (15.17)$$

As the applied tensile stress is the external variable for a given material having a crack of length $2c$, it is more appropriate to express the critical condition as a critical fracture stress, σ_c . Here, σ_c is the

critical value of stress required for the propagation of the flaw of length $2c$. This is the Griffith equation, a corner stone of modern fracture theory.

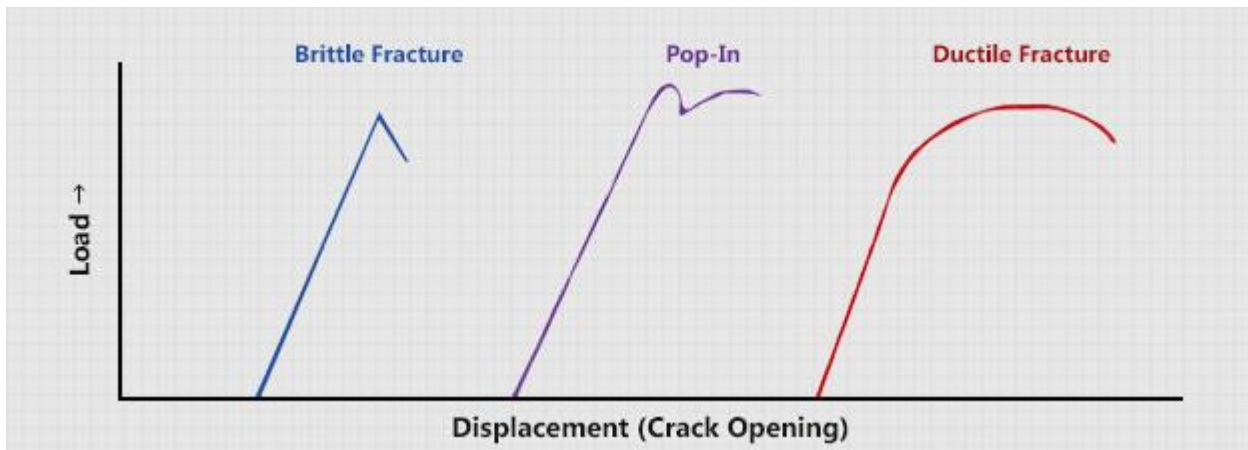
It is a go/no-go condition; that is, the flaw does not propagate until the critical value of stress is reached. Once the critical stress is applied to a brittle material, the pre-existing crack propagates spontaneously with a decrease in energy, or rather its rate of growth accelerates, since the strain-energy released as it lengthens is increasingly in excess of that required for the creation of new surfaces. This acceleration continues until the crack acquires a terminal velocity of the order of one-half the velocity of the longitudinal sound wave in the material.

The Griffith equation (15.17) produces an important result as it gives the value of critical stress required to propagate a crack in a brittle material as a function of the size of the micro-crack. It indicates that the fracture stress is inversely proportional to the square root of the crack length. For example, if the crack length increases by a factor of 9 decreases the fracture stress by one-third.

CTOD Test

Crack Tip Opening Displacement

The Crack Tip Opening Displacement or CTOD Test measures the resistance of a material to the propagation of a crack. CTOD is used on materials that can show some plastic deformation before failure occurs causing the tip to stretch open. Accurate measurement of this displacement is one of the essentials of the test. In the CTOD test the specimens are proportional. If the thickness is represented by 'A', then the depth will either be 'A', for a square cross section, or, '2A' for a rectangular cross section with the standard length being '4.6A'.

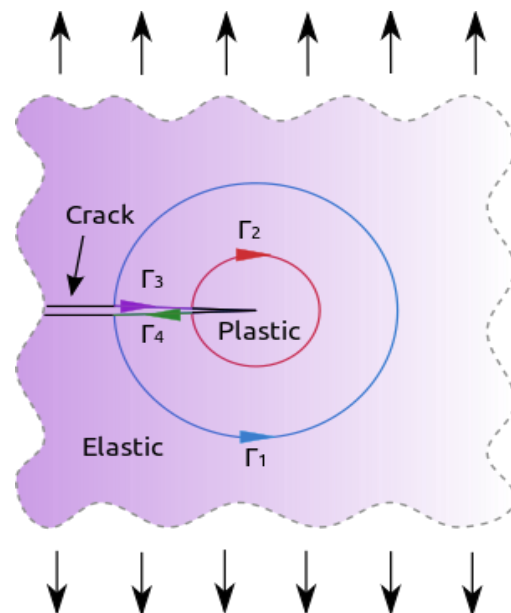


To prepare a specimen for a CTOD test, a notch is machined in the centre of the specimen and then an actual fatigue crack is carefully induced at the base of the notch. The crack must be long enough to pass through any area displaying plastic deformity caused by the machining process. The actual test is performed by placing the specimen in 3 point bending and accurately measuring the amount the crack

opens. For this purpose a strain gage is employed, mounted to a clip between two precisely placed knife edges at the mouth of the machined notch. The crack tip opening is plotted against the load applied. There are three basic types of fracture behavior with this test: brittle fracture, pop-in, and ductile. The first curve shows a brittle fracture with little or no plastic deformation. The curve shows a pop-in where the crack initiates in a brittle manner but is soon arrested by tougher more ductile material. This behavior can occur many times giving the curve a saw tooth appearance. And the third curve depicts a completely plastic or ductile behavior. Locating the notch correctly in the material being tested is important. A fatigue crack positioned incorrectly will not sample the required area thus invalidating the test. Polishing, etching and metallurgical examination are often used to provide the required accuracy in notch placement. These techniques may also be employed after the test to provide additional confirmation of the validity of the test. A low stress range is common when performing the fatigue cracking. Employing high stresses to speed up the process can cause large area of plastically deformed material to form ahead of the fatigue crack invalidating the test. Examination of the fatigue crack surface is necessary to determine the success or failure of the test. The length of the crack itself is accurately measured. If the length of the crack is not within the specified limits the test is invalid. If the crack is not in a single plane, or at an angle to the machined notch, or, if the crack is not in the proper region, the test is invalid.

J-integral

The J-integral represents a way to calculate the strain energy release rate, or work (energy) per unit fracture surface area, in a material. The theoretical concept of J-integral was developed in 1967 by G. P. Cherepanov and independently in 1968 by James R.



Relationship for CTOD and J-Integral

A modified line-plasticity model, involving concept of structured nonlinear zone coupled with the final stretch criterion governing the crack propagation, is used to show the effects of material strain-hardening and the redistribution of strain caused by an advancing quasi-static crack, on the essential parameters pertinent to a mathematical description of elasto-plastic fracture process including its ductile limit. The model links micro-structural and continuum aspects of ductile fracture occurring in dissipative solids equipped with an ability to strain-harden. Attention has been focused on the crack tip opening displacement (δ_t) and the J-integral, both associated with either stationary or quasi-static crack contained in a power-hardening material of the Ramberg–Osgood type. The ratios of δ_t and J for a stationary and moving crack are represented via closed-form solutions and then compared against the earlier numerical results of Shih (1981), based on the finite element analyses. Expressions derived here, apart from having a theoretical merit, address an issue of significant interest to the researchers involved in the field of the Experimental Fracture Mechanics.

4 Dynamic and Time-Dependent Fracture

In certain fracture problems, time is an important variable. At high loading rates, for example, inertia effects and material rate dependence can be significant. Metals and ceramics also exhibit rate-dependent deformation (creep) at temperatures that are close to the melting point of the material. The mechanical behavior of polymers is highly sensitive to strain rate, particularly above the glass transition temperature. In each of these cases, linear elastic and elastic-plastic fracture mechanics, which assume quasistatic, rate-independent deformation, are inadequate.

Early fracture mechanics researchers considered dynamic effects, but only for the special case of linear elastic material behavior. More recently, fracture mechanics has been extended to include time-dependent material behavior such as viscoplasticity and viscoelasticity. Most of these newer approaches are based on generalizations of the J contour integral.

This chapter gives an overview of time-dependent fracture mechanics. The treatment of this subject is far from exhaustive, but should serve as an introduction to a complex and rapidly developing field. The reader is encouraged to consult the published literature for a further background.

4.1 DYNAMIC FRACTURE AND CRACK ARREST

As any undergraduate engineering student knows, dynamics is more difficult than statics. Problems become more complicated when the equations of equilibrium are replaced by the equations of motion.

In the most general case, dynamic fracture mechanics contains three complicating features that are not present in LEFM and elastic-plastic fracture mechanics: inertia forces, rate-dependent material behavior, and reflected stress waves. Inertia effects are important when the load changes abruptly or the crack grows rapidly; a portion of the work that is applied to the specimen is converted to kinetic energy. Most metals are not sensitive to moderate variations in strain rate near ambient temperature, but the flow stress can increase appreciably when the strain rate increases by several orders of magnitude. The effect of rapid loading is even more pronounced in rate-sensitive materials such as polymers. When the load changes abruptly or the crack grows rapidly, stress waves propagate through the material and reflect off free surfaces, such as the specimen boundaries and the crack plane. Reflecting stress waves influence the local crack-tip stress and strain fields which, in turn, affect the fracture behavior.

In certain problems, one or more of the above effects can be ignored. If all three effects are neglected, the problem reduces to the quasistatic case.

The dynamic version of LEFM is termed *elastodynamic fracture mechanics*, where nonlinear material behavior is neglected, but inertia forces and reflected stress waves are incorporated when necessary. The theoretical framework of elastodynamic fracture mechanics is fairly well established, and practical applications of this approach are becoming more common. Extensive reviews of this subject have been published by Freund [1–5], Kanninen and Poplar [6], Rose [7], and others. Elastodynamic fracture mechanics has limitations, but is approximately valid in many cases. When the plastic zone is restricted to a small region near the crack tip in a dynamic problem, the stress-intensity approach, with some modifications, is still applicable.

Dynamic fracture analyses that incorporate nonlinear, time-dependent material behavior are a relatively recent innovation. A number of researchers have generalized the J integral to account for inertia and viscoplasticity [8–13].

There are two major classes of dynamic fracture problems: (1) fracture initiation as a result of rapid loading, and (2) rapid propagation of a crack. In the latter case, the crack propagation may initiate either by quasistatic or rapid application of a load; the crack may arrest after some amount of unstable propagation. Dynamic initiation, propagation, and crack arrest are discussed later in this chapter.

4.1.1 RAPID LOADING OF A STATIONARY CRACK

Rapid loading of a structure can come from a number of sources, but most often occurs as the result of impact with a second object (e.g., a ship colliding with an offshore platform or a missile striking its target). Impact loading is often applied in laboratory tests when a high strain rate is desired. The Charpy test [14], where a pendulum dropped from a fixed height fractures a notched specimen, is probably the most common dynamic mechanical test. Dynamic loading of a fracture mechanics specimen can be achieved through impact loading [15, 16], a controlled explosion near the specimen [17], or servo-hydraulic testing machines that are specially designed to impart high displacement rates. Chapter 7 describes some of the practical aspects of high rate fracture testing.

Figure 4.1 schematically illustrates a typical load-time response for dynamic loading. The load tends to increase with time, but oscillates at a particular frequency that depends on specimen geometry and material properties. Note that the loading rate is finite, i.e., a finite time is required to reach a particular load. The amplitude of the oscillations decreases with time, as kinetic energy is dissipated by the specimen. Thus, inertia effects are most significant at short times, and are minimal after sufficiently long times, where the behavior is essentially quasistatic.

Determining a fracture characterizing parameter, such as the stress-intensity factor or the J integral, for rapid loading can be very difficult. Consider the case where the plastic zone is confined to a small region surrounding the crack tip. The near-tip stress fields for high rate Mode I loading are given by Equation 4.1.

$$\sigma_{ij} = \frac{K_I(t)}{\sqrt{2\pi r}} \quad (4.1)$$

where (t) denotes a function of time. The angular functions f_{ij} are identical to the quasistatic case and are given in Table 2.1. The stress-intensity factor, which characterizes the amplitude of the elastic singularity, varies erratically in the early stages of loading. Reflecting stress waves that pass through the specimen constructively and destructively interfere with one another, resulting in a highly complex time-dependent stress distribution. The instantaneous K_I depends on the magnitude of the discrete stress waves that pass through the crack-tip region at that particular moment in time. When the discrete waves are significant, it is not possible to infer K_I from the remote loads.

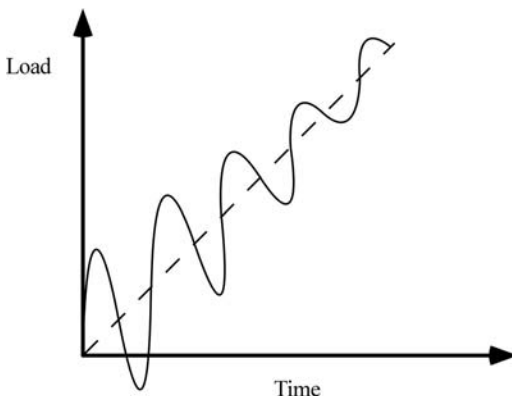


FIGURE 4.1 Schematic load-time response of a rapidly loaded structure.

Recent work by Nakamura et al. [18, 19] quantified inertia effects in laboratory specimens and showed that these effects can be neglected in many cases. They observed that the behavior of a dynamically loaded specimen can be characterized by a short-time response, dominated by discrete waves, and a long-time response that is essentially quasistatic. At intermediate times, global inertia effects are significant but local oscillations at the crack are small, because kinetic energy is absorbed by the plastic zone. To distinguish short-time response from long-time response, Nakamura et al. defined a *transition time* t_τ when the kinetic energy and the deformation energy (the energy absorbed by the specimen) are equal. Inertia effects dominate prior to the transition time, but the deformation energy dominates at times significantly greater than t_τ . In the latter case, a J -dominated field should exist near the crack tip and quasistatic relationships can be used to infer J from global load and displacement.

Since it is not possible to measure kinetic and deformation energies separately during a fracture mechanics experiment, Nakamura et al. developed a simple model to estimate the kinetic energy and the transition time in a three-point bend specimen (Figure 4.2). This model was based on the Bernoulli-Euler beam theory and assumed that the kinetic energy at early times was dominated by the elastic response of the specimen. Incorporating the known relationship between the load-line displacement and the strain energy in a three-point bend specimen leads to an approximate relationship for the ratio of kinetic to deformation energy:

$$\frac{E_k}{U} = \left(\Lambda \frac{W \dot{\Delta}(t)}{c_o \Delta(t)} \right)^2 \tag{4.2}$$

where

E_k = kinetic energy

U = deformation energy

W = specimen width

Δ = load line displacement

$\dot{\Delta}$ = displacement rate

c_o = longitudinal wave speed (i.e., the speed of sound) in a one-dimensional bar

Λ = geometry factor, which for the bend specimen is given by

$$\Lambda = \sqrt{\frac{SBEC}{W}} \tag{4.3}$$

where S is the span of the specimen.

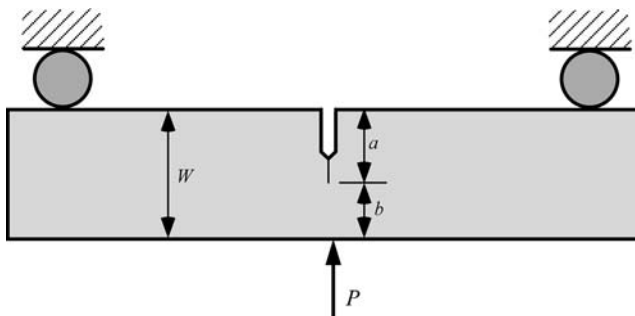


FIGURE 4.2 Three-point bend specimen.

The advantage of Equation (4.2) is that the displacement and displacement rate can be measured experimentally. The transition time is defined at the moment in the test when the ratio $E_k/U = 1$. In order to obtain an explicit expression for t_τ , it is convenient to introduce a dimensionless displacement coefficient D :

$$D = \frac{t\dot{\Delta}(t)}{\Delta(t)} \Big|_{t_\tau} \quad (4.4)$$

If, for example, the displacement varies with time as a power law: $\Delta = \beta t^\gamma$, then $D = \gamma$. Combining Equation (4.2) and Equation (4.4) and setting $E_k/U = 1$ leads to

$$t_\tau = D\Lambda \frac{W}{c_o} \quad (4.5)$$

Nakamura et al. [18, 19] performed a dynamic finite element analysis on a three-point bend specimen in order to evaluate the accuracy of Equation (4.2) and Equation (4.5). Figure 4.3 compares the E_k/U ratio computed from a finite element analysis with that determined from the experiment and Equation (4.2). The horizontal axis is a dimensionless time scale, and c_1 is the longitudinal wave speed in an unbounded solid. The ratio W/c_1 is an estimate of the time required for a stress wave to traverse the width of the specimen. Based on Equation (4.2) and the experiment, $t_\tau c_1/W \approx 28$ (or $t_\tau c_o/H \approx 24$), while the finite element analysis estimated $t_\tau c_1/W \approx 27$. Thus the simple model agrees quite well with a more detailed analysis.

The simple model was based on the global kinetic energy and did not consider discrete stress waves. Thus the model is only valid after stress waves have traversed the width of the specimen several times. This limitation does not affect the analysis of the transition time, since stress waves have made approximately 27 passes when t_τ is reached. Note, in Figure 4.3, that the simple model agrees very well with the finite element analysis when $t c_1/W > 20$.

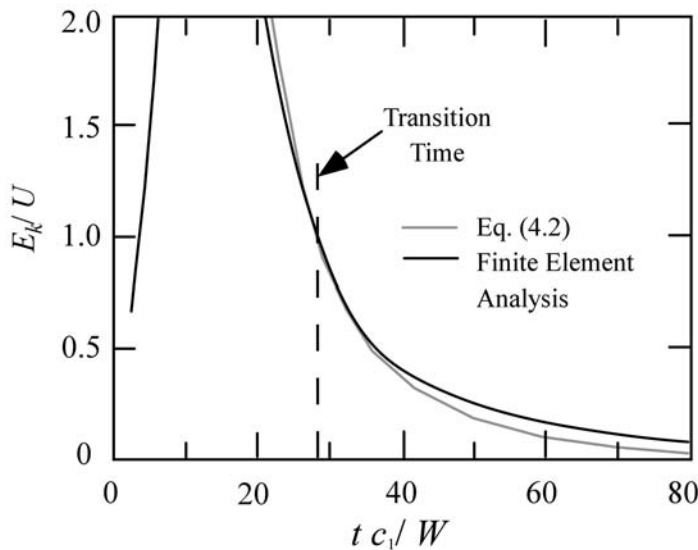


FIGURE 4.3 Ratio of kinetic to stress work energy in a dynamically loaded three-point bend specimen. Taken from Nakamura, T., Shih, C.F., and Freund, L.B., “Three-Dimensional Transient Analysis of a Dynamically Loaded Three-Point-Bend Ductile Fracture Specimen.” ASTM STP 995, Vol. I, American Society for Testing and Materials, Philadelphia, PA, 1989, pp. 217–241.

When $t \gg t_\tau$, inertia effects are negligible and quasistatic models should apply to the problem. Consequently, the J integral for a deeply cracked bend specimen at long times can be estimated by

$$J_{dc} = \frac{2}{Bb} \int_0^{\Omega(t^*)} M(t) d\Omega(t) \tag{4.6}$$

where

- B = plate thickness
- b = uncracked ligament length
- M = applied moment on the ligament
- Ω = angle of rotation
- t^* = current time

Equation (4.6), which was originally published by Rice et al. [20], is derived in Section 3.2.5.

Nakamura et al. [19] performed a three-dimensional dynamic elastic-plastic finite element analysis on a three-point bend specimen in order to determine the range of applicability of Equation (4.6). They evaluated a dynamic J integral (see Section 4.1.3) at various thickness positions and observed a through-thickness variation of J that is similar to Figure 3.36. They computed a nominal J that averaged the through-thickness variations and compared this value with J_{dc} . The results of this exercise are plotted in Figure 4.4. At short times, the average dynamic J is significantly lower than the J computed from the quasistatic relationship. For $t > 2t_\tau$, the J_{dc}/J_{ave} reaches a constant value that is slightly greater than 1. The modest discrepancy between J_{dc} and J_{ave} at long times is probably due to three-dimensional effects rather than dynamic effects (Equation (4.6) is essentially a two-dimensional formula).

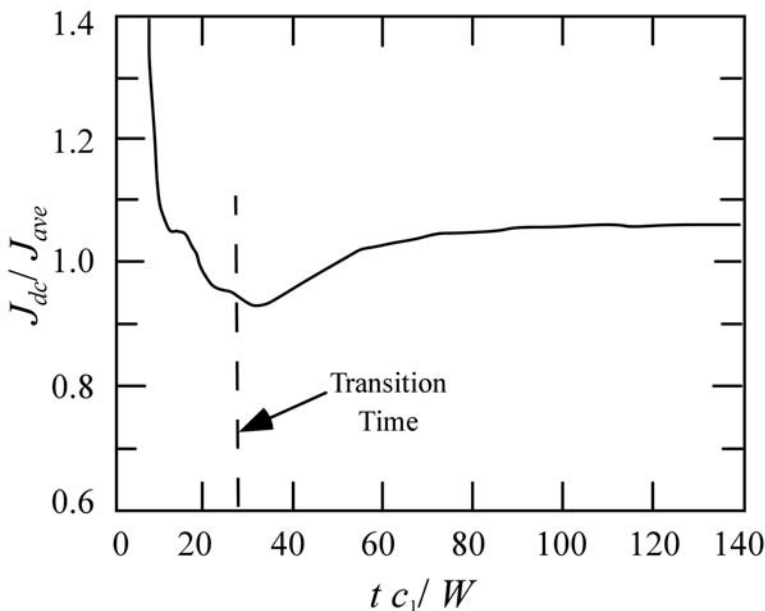


FIGURE 4.4 Ratio of J computed from Equation (4.6) to the through-thickness average J computed from a three-dimensional dynamic finite element analysis.

According to Figure 4.4, Equation (4.6) provides a good estimate of J in a high-rate test at times greater than approximately twice the transition time. It follows that if the fracture initiation occurs after $2t_t$, the critical value of J obtained from Equation (4.6) is a measure of the fracture toughness for high-rate loading. If small-scale yielding assumptions apply, the critical J can be converted to an equivalent K_{Ic} through Equation (3.18).

Given the difficulties associated with defining a fracture parameter in the presence of inertia forces and reflected stress waves, it is obviously preferable to apply Equation (4.6) whenever possible. For a three-point bend specimen with $W = 50$ mm, the transition time is approximately $300 \mu\text{s}$ [19]. Thus the quasistatic formula can be applied as long as fracture occurs after $\sim 600 \mu\text{s}$. This requirement is relatively easy to meet in impact tests on ductile materials [15, 16]. For more brittle materials, the transition-time requirement can be met by decreasing the displacement rate or the width of the specimen.

The transition-time concept can be applied to other configurations by adjusting the geometry factor in Equation (4.2). Duffy and Shih [17] have applied this approach to dynamic fracture toughness measurement in notched round bars. Small round bars have proved to be suitable for the dynamic testing of brittle materials such as ceramics, where the transition time must be small.

If the effects of inertia and reflected stress waves can be eliminated, one is left with the rate-dependent material response. The transition-time approach allows material rate effects to be quantified independent of inertia effects. High strain rates tend to elevate the flow stress of the material. The effect of flow stress on fracture toughness depends on the failure mechanism. High strain rates tend to decrease cleavage resistance, which is stress controlled. Materials whose fracture mechanisms are strain controlled often see an increase in toughness at high loading rates because more energy is required to reach a given strain value.

Figure 4.5 shows the fracture toughness data for a structural steel at three loading rates [21]. The critical K_I values were determined from quasistatic relationships. For a given loading rate, the fracture toughness increases rapidly with temperature at the onset of the ductile-brittle transition. Note that increasing the loading rate has the effect of shifting the transition to higher temperatures. Thus, at a constant temperature, fracture toughness is highly sensitive to strain rate.

The effect of the loading rate on the fracture behavior of a structural steel on the upper shelf of toughness is illustrated in Figure 4.6. In this instance, the strain rate has the opposite effect from Figure 4.5, because ductile fracture of metals is primarily strain controlled. The J integral at a given amount of crack extension is elevated by high strain rates.

4.1.2 RAPID CRACK PROPAGATION AND ARREST

When the driving force for crack extension exceeds the material resistance, the structure is unstable, and rapid crack propagation occurs. Figure 4.7 illustrates a simple case, where the (quasistatic) energy release rate increases linearly with the crack length and the material resistance is constant. Since the first law of thermodynamics must be obeyed even by an unstable system, the excess energy, denoted by the shaded area in Figure 4.7, does not simply disappear, but is converted into kinetic energy. The magnitude of the kinetic energy dictates the crack speed.

In the quasistatic case, a crack is stable if the driving force is less than or equal to the material resistance. Similarly, if the energy available for an incremental extension of a rapidly propagating crack falls below the material resistance, the crack arrests. Figure 4.8 illustrates a simplified scenario for crack arrest. Suppose that cleavage fracture initiates when $K_I = K_{Ic}$. The resistance encountered by a rapidly propagating cleavage crack is less than for cleavage initiation, because plastic deformation at the moving crack tip is suppressed by the high local strain rates. If the structure has a falling driving force curve, it eventually crosses the resistance curve. Arrest does not occur at this point, however, because the structure contains kinetic energy that can be converted to fracture

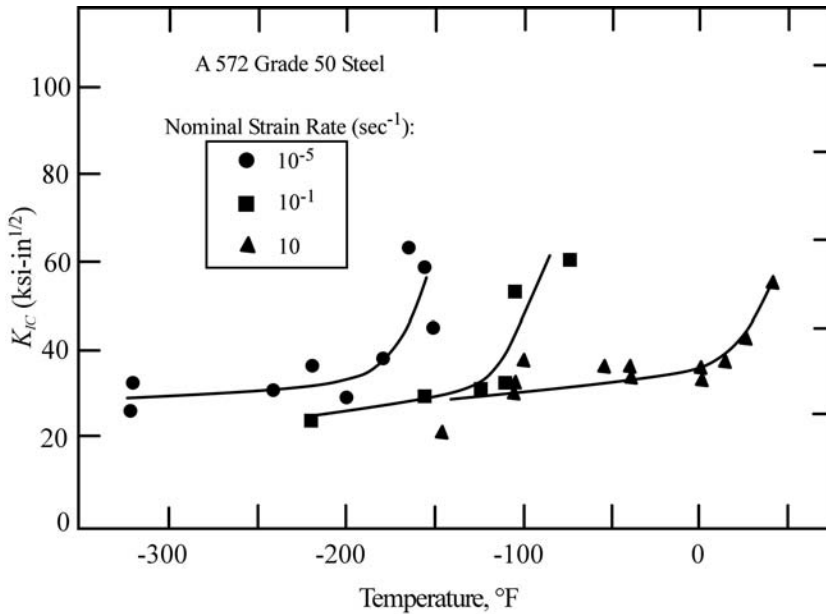


FIGURE 4.5 Effect of loading rate on the cleavage fracture toughness of a structural steel. Taken from Barsom, J.M., “Development of the AASHTO Fracture Toughness Requirements for Bridge Steels.” *Engineering Fracture Mechanics*, Vol. 7, 1975, pp. 605–618.

energy. Arrest occurs below the resistance curve, after most of the available energy has been dissipated. The apparent arrest toughness K_{Ia} is less than the true material resistance K_{IA} . The difference between K_{Ia} and K_{IA} is governed by the kinetic energy created during crack propagation; K_{IA} is a material property, but K_{Ia} depends on geometry.

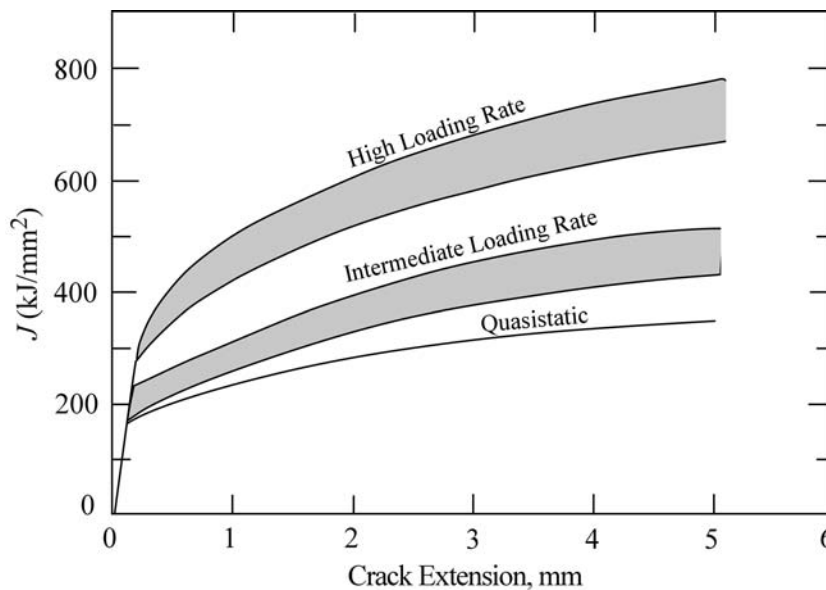


FIGURE 4.6 Effect of loading rate on the J - R curve behavior of HY80 steel. Taken from Joyce, J.A. and Hacket, E.M., “Dynamic J - R Curve Testing of a High Strength Steel Using the Multispecimen and Key Curve Techniques.” ASTM STP 905, American Society for Testing and Materials, Philadelphia, PA, 1984, pp. 741–774.

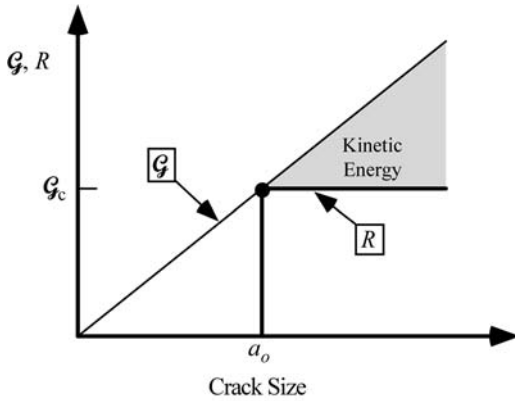


FIGURE 4.7 Unstable crack propagation, which results in the generation of kinetic energy.

Figure 4.7 and Figure 4.8 compare material resistance with *quasistatic* driving force curves. That is, these curves represent K_I and \mathcal{G} values computed with the procedures described in Chapter 2. Early researchers [22–26] realized that the crack-driving force should incorporate the effect of kinetic energy. The Griffith-Irwin energy balance (Section 2.3 and Section 2.4) can be modified to include kinetic energy, resulting in a dynamic definition of the energy release rate:

$$\mathcal{G}(t) = \frac{dF}{dA} - \frac{dU}{dA} - \frac{dE_k}{dA} \tag{4.7}$$

where F is the work done by external forces and A is the crack area. Equation (4.7) is consistent with the original Griffith approach, which is based on the first law of thermodynamics. The kinetic energy must be included in a general statement of the first law; Griffith implicitly assumed that $E_k = 0$.

4.1.2.1 Crack Speed

Mott [22] applied dimensional analysis to a propagating crack in order to estimate the relationship between kinetic energy and crack speed. For a through crack of length $2a$ in an infinite plate in tension, the displacements must be proportional to the crack size, since a is the only relevant length

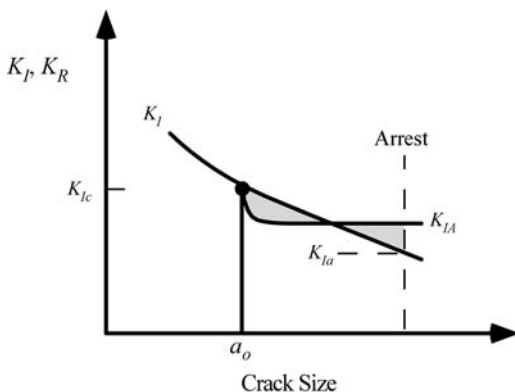


FIGURE 4.8 Unstable crack propagation and arrest with a falling driving-force curve. The apparent arrest toughness K_{Ia} is slightly below the true material resistance K_{Ic} due to excess kinetic energy.

dimension. Assuming the plate is elastic, the displacements must also be proportional to the nominal applied strain; thus

$$u_x = \alpha_x a \frac{\sigma}{E} \quad \text{and} \quad u_y = \alpha_y a \frac{\sigma}{E} \quad (4.8)$$

where α_x and α_y are dimensionless constants. (Note that quantitative estimates for α_x and α_y near the crack tip in the quasistatic case can be obtained by applying the relationships in Table 2.2.) The kinetic energy is equal to half the mass times the velocity squared. Therefore, E_k for the cracked plate (assuming a unit thickness) is given by

$$E_k = \frac{1}{2} \rho a^2 V^2 \left(\frac{\sigma}{E} \right)^2 \iint (\alpha_x^2 + \alpha_y^2) dx dy \quad (4.9)$$

where ρ is the mass density of the material and $V(=\dot{a})$ is the crack speed. Assuming the integrand depends only on position,¹ E_k can be written in the following form:

$$E_k = \frac{1}{2} k \rho a^2 V^2 \left(\frac{\sigma}{E} \right)^2 \quad (4.10)$$

where k is a constant. Applying the modified Griffith energy balance (Equation (4.7)) gives

$$\mathcal{G}(t) = \frac{1}{2} \frac{d}{da} \left[\frac{\pi \sigma^2 a^2}{E} - \frac{k}{2} \rho a^2 V^2 \left(\frac{\sigma}{E} \right)^2 \right] = 2w_f \quad (4.11)$$

where w_f is the work of fracture, defined in Chapter 2; in the limit of an ideally brittle material, $w_f = \gamma_s$, the surface energy. Note that Equation (4.11) assumes a flat R curve (constant w_f). At initiation, the kinetic energy term is not present, and the initial crack length a_o can be inferred from Equation (2.22):

$$a_o = \frac{2Ew_f}{\pi \sigma^2} \quad (4.12)$$

Substituting Equation (4.12) into Equation (4.11) and solving for V leads to

$$V = \sqrt{\frac{2\pi}{k} c_o} \left(1 - \frac{a_o}{a} \right) \quad (4.13)$$

where $c_o = \sqrt{E/\rho}$, the speed of sound for one-dimensional wave propagation. Mott [22] actually obtained a somewhat different relationship from Equation (4.13), because he solved Equation (4.11) by making the erroneous assumption that $dV/da = 0$. Dulaney and Brace [27] and Berry [28] later corrected the Mott analysis and derived Equation (4.13).

Roberts and Wells [29] obtained an estimate for k by applying the Westergaard stress function (Appendix 2.3) for this configuration. After making a few assumptions, they showed that $\sqrt{2\pi/k} \approx 0.38$.

¹ In a rigorous dynamic analysis, α_x and α_y and thus k depend on the crack speed.

According to Equation (4.13) and the Roberts and Wells analysis, the crack speed reaches a limiting value of $0.38c_o$ when $a \gg a_o$. This estimate compares favorably with measured crack speeds in metals, which typically range from 0.2 to $0.4c_o$ [30].

Freund [2–4] performed a more detailed numerical analysis of a dynamically propagating crack in an infinite body and obtained the following relationship:

$$V = c_r \left(1 - \frac{a_o}{a} \right) \quad (4.14)$$

where c_r is the Raleigh (surface) wave speed. For Poisson's ratio = 0.3, the c_r/c_o ratio = 0.57. Thus the Freund analysis predicts a larger limiting crack speed than the Roberts and Wells analysis. The limiting crack speed in Equation (4.14) can be argued on physical grounds [26]. For the special case where $w_f = 0$, a propagating crack is merely a disturbance on a free surface that must move at the Raleigh wave velocity. In both Equation (4.13) and Equation (4.14), the limiting velocity is independent of the fracture energy; thus the maximum crack speed should be c_r for all w_f .

Experimentally observed crack speeds do not usually reach c_r . Both the simple analysis that resulted in Equation (4.13) and Freund's more detailed dynamic analysis assumed that the fracture energy does not depend on crack length or crack speed. The material resistance actually increases with crack speed, as discussed below. The good agreement between experimental crack velocities and the Roberts and Wells estimate of $0.38c_o$ is largely coincidental.

4.1.2.2 Elastodynamic Crack-Tip Parameters

The governing equation for Mode I crack propagation under elastodynamic conditions can be written as

$$K_I(t) = K_{ID}(V) \quad (4.15)$$

where K_I is the instantaneous stress intensity and K_{ID} is the material resistance to crack propagation, which depends on the crack velocity. In general, $K_I(t)$ is not equal to the static stress-intensity factor, as defined in Chapter 2. A number of researchers [8–10, 31–33] have obtained a relationship for the dynamic stress intensity of the form

$$K_I(t) = \mathbf{k}(V)K_I(0) \quad (4.16)$$

where \mathbf{k} is a universal function of crack speed and $K_I(0)$ is the static stress-intensity factor. The function $\mathbf{k}(V) = 1.0$ when $V = 0$, and decreases to zero as V approaches the Raleigh wave velocity. An approximate expression for \mathbf{k} was obtained by Rose [34]:

$$\mathbf{k}(V) \approx \left(1 - \frac{V}{c_r} \right) \sqrt{1 - hV} \quad (4.17)$$

where h is a function of the elastic wave speeds and can be approximated by

$$h \approx \frac{2}{c_1} \left(\frac{c_2}{c_r} \right)^2 \left[1 - \left(\frac{c_2}{c_1} \right) \right]^2 \quad (4.18)$$

where c_1 and c_2 are the longitudinal and shear wave speeds, respectively.

Equation (4.16) is valid only at short times or in infinite bodies. This relationship neglects reflected stress waves, which can have a significant effect on the local crack-tip fields. Since the crack speed is proportional to the wave speed, Equation (4.16) is valid as long as the length of crack propagation ($a - a_o$) is small compared to the specimen dimensions, because reflecting stress waves will not have had time to reach the crack tip (Example 4.1). In finite specimens where stress waves reflect back to the propagating crack tip, the dynamic stress intensity must be determined experimentally or numerically on a case-by-case basis.

EXAMPLE 4.1

Rapid crack propagation initiates in a deeply notched specimen with an initial ligament b_o (Figure 4.9). Assuming the average crack speed = $0.2 c_1$, estimate how far the crack will propagate before it encounters a reflected longitudinal wave.

Solution: At the moment the crack encounters the first reflected wave, the crack has traveled a distance Δa , while the wave has traveled $2b_o - \Delta a$. Equating the travel times gives

$$= \frac{\Delta a}{0.2c_1} = \frac{2b_o - \Delta a}{c_1}$$

thus,

$$\Delta a = \frac{b_o}{3}$$

Equation (4.16) is valid in this case as long as the crack extension is less than $b_o/3$ and the plastic zone is small compared to b_o .

For an infinite body or short times, Freund [10] showed that the dynamic energy release rate could be expressed in the following form:

$$\mathcal{G}(t) = g(V)\mathcal{G}(0) \tag{4.19}$$

where g is a universal function of crack speed that can be approximated by

$$g(V) \approx 1 - \frac{V}{c_r} \tag{4.20}$$

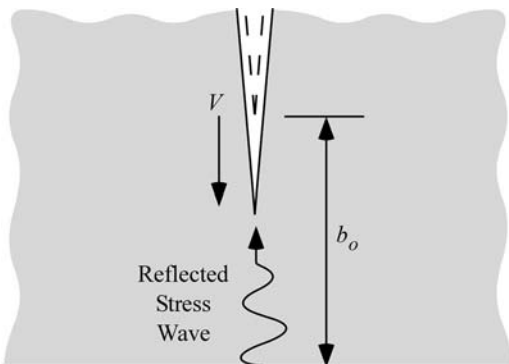


FIGURE 4.9 Propagating crack encountering a reflected stress wave.

Combining Equation (4.16)–(4.20) with Equation (2.51) gives

$$\mathcal{G}(t) = A(V) \frac{K_I^2(t)}{E'} \quad (4.21)$$

where

$$A(V) \approx \left[\left(1 - \frac{V}{c_r} \right) (1 - hV) \right]^{-1} \quad (4.22)$$

Thus the relationship between K_I and \mathcal{G} depends on crack speed. A more accurate (and more complicated) relationship for $A(V)$ is given in Appendix 4.1.

When the plastic zone ahead of the propagating crack is small, $K_I(t)$ uniquely defines the crack-tip stress, strain, and displacement fields, but the angular dependence of these quantities is different from the quasistatic case. For example, the stresses in the elastic singularity zone are given by [32, 33, 35]

$$\sigma_{ij} = \frac{K_I(t)}{\sqrt{2\pi r}} f_{ij}(\theta, V) \quad (4.23)$$

The function f_{ij} reduces to the quasistatic case (Table 2.1) when $V = 0$. Appendix 4.1 outlines the derivation of Equation (4.23) and gives specific relationships for f_{ij} in the case of rapid crack propagation. The displacement functions also display an angular dependence that varies with V . Consequently, α_x and α_y in Equation (4.9) must depend on crack velocity as well as position, and the Mott analysis is not rigorously correct for dynamic crack propagation.

4.1.2.3 Dynamic Toughness

As Equation (4.15) indicates, the dynamic stress intensity is equal to K_{ID} , the dynamic material resistance, which depends on crack speed. This equality permits experimental measurements of K_{ID} .

Dynamic propagation toughness can be measured as a function of crack speed by means of high-speed photography and optical methods, such as photoelasticity [36, 37] and the method of caustics [38]. Figure 4.10 shows photoelastic fringe patterns for dynamic crack propagation in Homalite 100 [37]. Each fringe corresponds to a contour of maximum shear stress. Sanford and Dally [36] describe procedures for inferring stress intensity from photoelastic patterns.

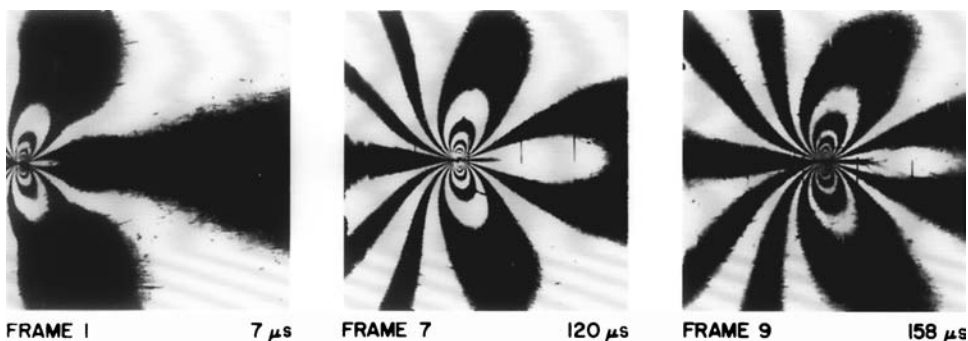


FIGURE 4.10 Photoelastic fringe patterns for a rapidly propagating crack in Homalite 100. Photograph provided by R. Chona. Taken from Chona, R., Irwin, G.R., and Shukla, A., “Two and Three Parameter Representation of Crack Tip Stress Fields.” *Journal of Strain Analysis*, Vol. 17, 1982, pp. 79–86.

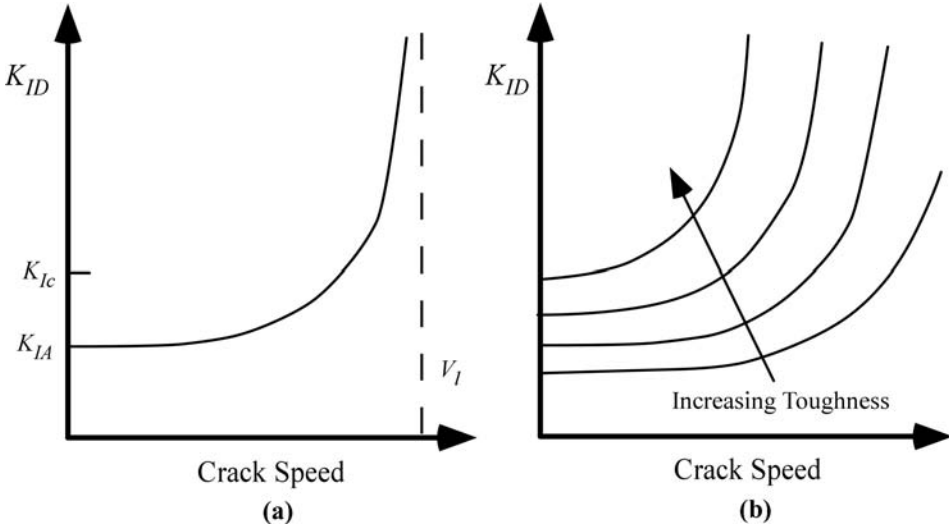


FIGURE 4.11 Schematic K_{ID} -crack speed curves: (a) effect of crack speed on K_{ID} and (b) effect of material toughness.

Figure 4.11 illustrates the typical variation of K_{ID} with crack speed. At low speeds, K_{ID} is relatively insensitive to V , but K_{ID} increases asymptotically as V approaches a limiting value. Figure 4.12 shows K_{ID} data for 4340 steel published by Rosakis and Freund [39].

In the limit of $V = 0$, $K_{ID} = K_{IA}$, the arrest toughness of the material. In general, $K_{IA} < K_{IC}$, the quasistatic initiation toughness. When a stationary crack in an elastic-plastic material is loaded monotonically, the crack-tip blunts and a plastic zone forms. A propagating crack, however, tends to be sharper and has a smaller plastic zone than a stationary crack. Consequently, more energy is required to initiate fracture from a stationary crack than is required to maintain the propagation of a sharp crack.

The crack-speed dependence of K_{ID} can be represented by an empirical equation of the form

$$K_{ID} = \frac{K_{IA}}{1 - \left(\frac{V}{V_l}\right)^m} \tag{4.24}$$

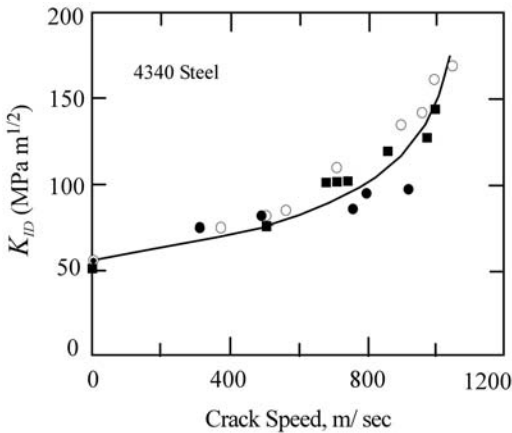


FIGURE 4.12 Experimental K_{ID} vs. crack speed data for 4340 steel. Taken from Rosakis, A.J. and Freund, L.B., “Optical Measurement of the Plane Strain Concentration at a Crack Tip in a Ductile Steel Plate.” *Journal of Engineering Materials Technology*, Vol. 104, 1982, pp. 115–120.

where V_l is the limiting crack speed in the material and m is an experimentally determined constant. As Figure 4.11(b) illustrates, K_{IA} increases and V_l decreases with increasing material toughness. The trends in Figure 4.11(a) and Figure 4.11(b) have not only been observed experimentally, but have also been obtained by numerical simulation [40, 41]. The upturn in propagation toughness at high crack speeds is apparently caused by local inertia forces in the plastic zone.

4.1.2.4 Crack Arrest

Equation (4.15) defines the conditions for rapid crack advance. If, however, $K_I(t)$ falls below the minimum K_{ID} value for a finite length of time, propagation cannot continue, and the crack arrests. There are a number of situations that might lead to crack arrest. Figure 4.8 illustrates one possibility: If the driving force decreases with crack extension, it may eventually be less than the material resistance. Arrest is also possible when the material resistance increases with crack extension. For example, a crack that initiates in a brittle region of a structure, such as a weld, may arrest when it reaches a material with higher toughness. A temperature gradient in a material that exhibits a ductile-brittle transition is another case where the toughness can increase with position: A crack may initiate in a cold region of the structure and arrest when it encounters warmer material with a higher toughness. An example of this latter scenario is a pressurized thermal shock event in a nuclear pressure vessel [42].

In many instances, it is not possible to guarantee with absolute certainty that an unstable fracture will not initiate in a structure. Transient loads, for example, may occur unexpectedly. In such instances crack arrest can be the second line of defense. Thus, the crack arrest toughness K_{IA} is an important material property.

Based on Equation (4.16), one can argue that $K_I(t)$ at arrest is equivalent to the quasistatic value, since $V = 0$. Thus it should be possible to infer K_{IA} from a quasistatic calculation based on the load and crack length at arrest. This quasistatic approach to arrest is actually quite common, and is acceptable in many practical situations. Chapter 7 describes a standardized test method for measuring crack-arrest toughness that is based on quasistatic assumptions.

However, the quasistatic arrest approach must be used with caution. Recall that Equation (4.16) is valid only for infinite structures or short crack jumps, where reflected stress waves do not have sufficient time to return to the crack tip. When reflected stress wave effects are significant, Equation (4.16) is no longer valid, and a quasistatic analysis tends to give misleading estimates of the arrest toughness. Quasistatic estimates of arrest toughness are sometimes given the designation K_{Ia} ; for short crack jumps $K_{Ia} = K_{IA}$.

The effect of stress waves on the apparent arrest toughness K_{Ia} was demonstrated dramatically by Kalthoff et al. [43], who performed dynamic propagation and arrest experiments on wedge-loaded double cantilever beam (DCB) specimens. Recall from Example 2.3 that the DCB specimen exhibits a falling driving-force curve in displacement control. Kalthoff et al. varied the K_I at initiation by varying the notch-root radius. When the crack was sharp, fracture initiated slightly above K_{IA} and arrested after a short crack jump; the length of crack jump increased with the notch-tip radius.

Figure 4.13 is a plot of the Kalthoff et al. results. For the shortest crack jump, the true arrest toughness and the apparent quasistatic value coincide, as expected. As the length of crack jump increases, the discrepancy between the true arrest and the quasistatic estimate increases, with $K_{IA} > K_{Ia}$. Note that K_{IA} appears to be a material constant but K_{Ia} varies with the length of crack propagation. Also note that the dynamic stress intensity during crack growth is considerably different from the quasistatic estimate of K_I . Kobayashi et al. [44] obtained similar results.

A short time after arrest, the applied stress intensity reaches K_{Ia} , the quasistatic value. Figure 4.14 shows the variation of K_I after arrest in one of the Kalthoff et al. experiments. When the crack arrests, $K_I = K_{IA}$, which is greater than K_{Ia} . Figure 4.14 shows that the specimen “rings down” to K_{Ia} after $\sim 2000 \mu\text{s}$. The quasistatic value, however, is not indicative of the true material-arrest properties.

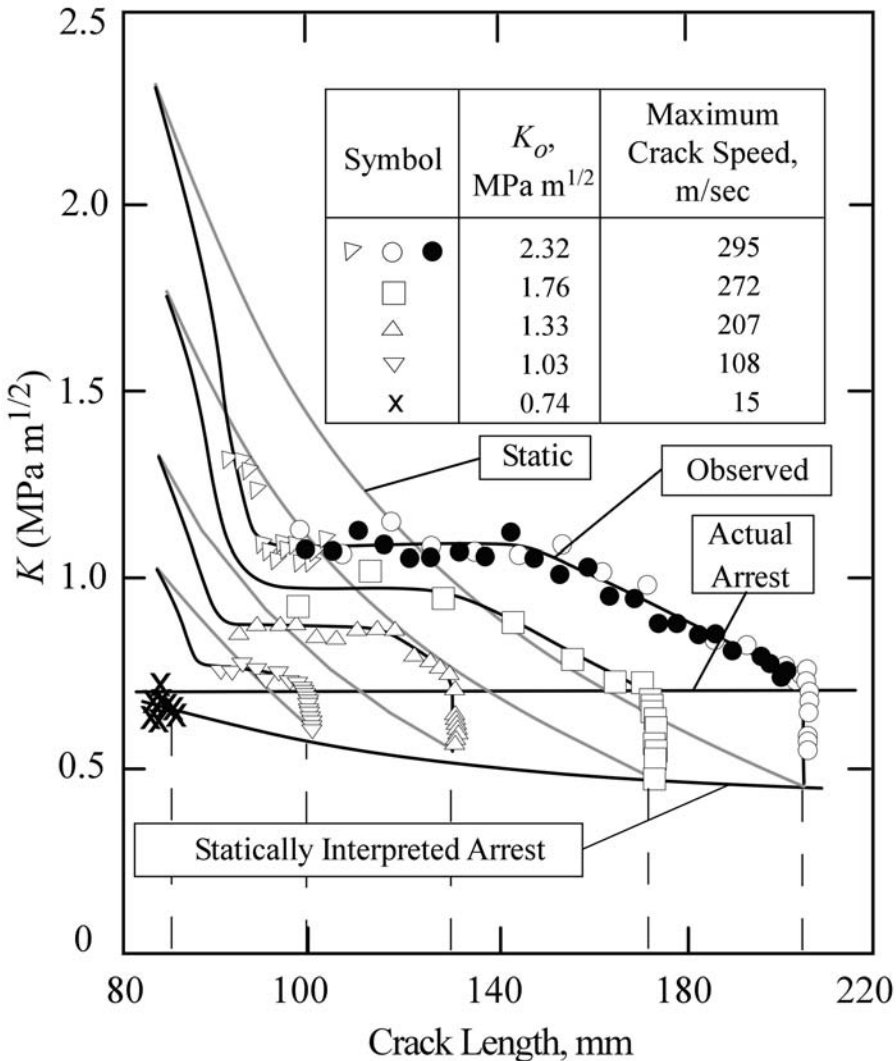


FIGURE 4.13 Crack arrest experiments on wedge-loaded DCB Araldite B specimens. The statically interpreted arrest toughness underestimates the true K_{Ia} of the material; this effect is most pronounced for long crack jumps. Taken from Kalthoff, J.F., Beinart, J., and Winkler, S., “Measurement of Dynamic Stress Intensity Factors for Fast Running and Arresting Cracks in Double-Cantilever Beam Specimens.” ASTM STP 627, American Society for Testing and Materials, Philadelphia, PA, 1977, pp. 161–176.

Recall the schematic in Figure 4.8, where it was argued that arrest, when quantified by the quasistatic stress intensity, would occur below the true arrest toughness K_{Ia} , because of the kinetic energy in the specimen. This argument is a slight oversimplification, but it leads to the correct qualitative conclusion.

The DCB specimen provides an extreme example of reflected stress wave effects; the specimen design is such that stress waves can traverse the width of the specimen and return to the crack tip in a very short time. In many structures, the quasistatic approach is approximately valid, even for relatively long crack jumps. In any case, K_{Ia} gives a lower bound estimate of K_{Ia} , and thus is conservative in most instances.

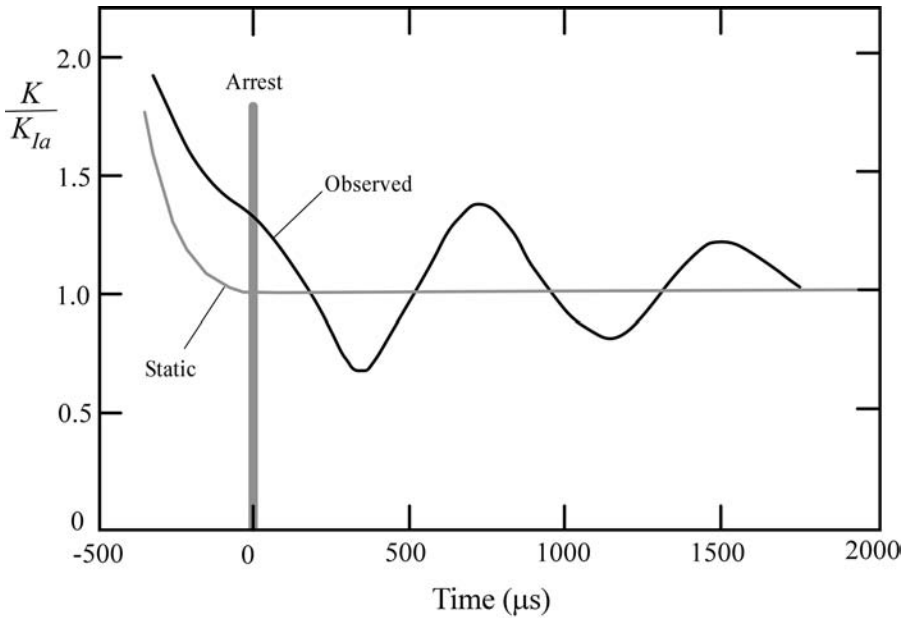


FIGURE 4.14 Comparison of dynamic measurements of stress intensity with static calculations for a wedge loaded DCB Araldite B specimen. Taken from Kalthoff, J.F., Beinart, J., and Winkler, S., “Measurement of Dynamic Stress Intensity Factors for Fast Running and Arresting Cracks in Double-Cantilever Beam Specimens.” ASTM STP 627, American Society for Testing and Materials, Philadelphia, PA, 1977, pp. 161–176.

4.1.3 DYNAMIC CONTOUR INTEGRALS

The original formulation of the J contour integral is equivalent to the nonlinear elastic energy release rate for quasistatic deformation. By invoking a more general definition of energy release rate, it is possible to incorporate dynamic effects and time-dependent material behavior into the J integral.

The energy release rate is usually defined as the energy released from the body per unit crack advance. A more precise definition [11] involves the work input into the crack tip. Consider a vanishingly small contour Γ around the tip of a crack in a two-dimensional solid (Figure 4.15). The energy release rate is equal to the energy flux into the crack tip, divided by the crack speed:

$$J = \frac{\mathcal{F}}{V} \tag{4.25}$$

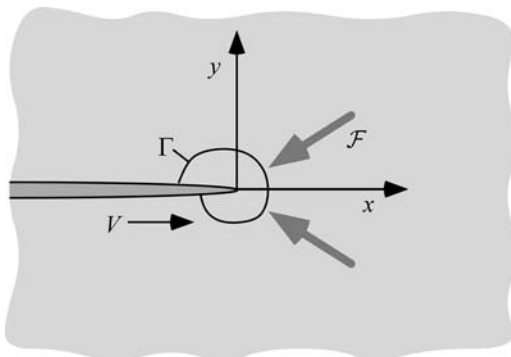


FIGURE 4.15 Energy flux into a small contour at the tip of a propagating crack.

where \mathcal{F} is the energy flux into the area bounded by Γ . The generalized energy release rate, including inertia effects, is given by

$$J = \lim_{\Gamma \rightarrow 0} \int_{\Gamma} \left[(w + T)dy - \sigma_{ij} n_j \frac{\partial u_i}{\partial x} ds \right] \quad (4.26)$$

where w and T are the stress work and kinetic energy densities defined as

$$w = \int_0^{\epsilon_{ij}} \sigma_{ij} d\epsilon_{ij} \quad (4.27)$$

and

$$T = \frac{1}{2} \rho \frac{\partial u_i}{\partial t} \frac{\partial u_i}{\partial t} \quad (4.28)$$

Equation (4.26) has been published in a variety of forms by several researchers [8–12]. Appendix 4.2 gives a derivation of this relationship.

Equation (4.26) is valid for time-dependent as well as history-dependent material behavior. When evaluating J for a time-dependent material, it may be convenient to express w in the following form:

$$w = \int_{t_0}^{t'} \sigma_{ij} \dot{\epsilon}_{ij} dt \quad (4.29)$$

where $\dot{\epsilon}_{ij}$ is the strain rate.

Unlike the conventional J integral, the contour in Equation (4.26) cannot be chosen arbitrarily. Consider, for example, a dynamically loaded cracked body with stress waves reflecting off free surfaces. If the integral in Equation (4.26) were computed at two arbitrary contours a finite distance from the crack tip and a stress wave passed through one contour but not the other, the values of these integrals would normally be different for the two contours. Thus, the generalized J integral is not path independent, except in the immediate vicinity of the crack tip. If, however, $T = 0$ at all points in the body, the integrand in Equation (4.26) reduces to the form of the original J integral. In the latter case, the path-independent property of J is restored if w displays the property of an elastic potential (see Appendix 4.2).

The form of Equation (4.26) is not very convenient for numerical calculations, since it is extremely difficult to obtain adequate numerical precision from a contour integration very close to the crack tip. Fortunately, Equation (4.26) can be expressed in a variety of other forms that are more conducive to numerical analysis. The energy release rate can also be generalized to three dimensions. The results in Figure 4.3 and Figure 4.4 are obtained from a finite element analysis that utilized alternate forms of Equation (4.26). Chapter 12 discusses the numerical calculations of J for both quasistatic and dynamic loading.

4.2 CREEP CRACK GROWTH

Components that operate at high temperatures relative to the melting point of the material may fail by the slow and stable extension of a macroscopic crack. Traditional approaches to design in the creep regime apply only when creep and material damage are uniformly distributed. Time-dependent fracture mechanics approaches are required when creep failure is controlled by a dominant crack in the structure.

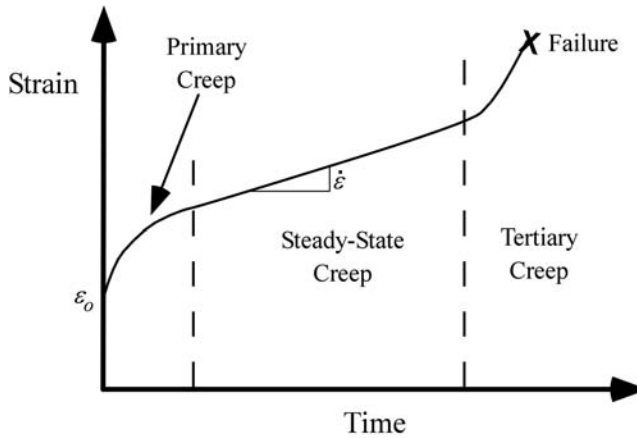


FIGURE 4.16 Schematic creep behavior of a material subject to a constant stress.

Figure 4.16 illustrates the typical creep response of a material subject to constant stress. Deformation at high temperatures can be divided into four regimes: instantaneous (elastic) strain, primary creep, secondary (steady state) creep, and tertiary creep. The elastic strain occurs immediately upon application of the load. As discussed in the previous section on dynamic fracture, the elastic stress-strain response of a material is not instantaneous (i.e., it is limited by the speed of sound in the material), but it can be viewed as such in creep problems, where the time scale is usually measured in hours. Primary creep dominates at short times after the application of the load; the strain rate decreases with time, as the material strain hardens. In the secondary creep stage, the deformation reaches a steady state, where strain hardening and strain softening are balanced; the creep rate is constant in the secondary stage. In the tertiary stage, the creep rate accelerates, as the material approaches ultimate failure. Microscopic failure mechanisms, such as grain boundary cavitation, nucleate in this final stage of creep.

During the growth of a macroscopic crack at high temperatures, all four types of creep response can occur simultaneously in the most general case (Figure 4.17). The material at the tip of a growing crack is in the tertiary stage of creep, since the material is obviously failing locally. The material may be elastic remote from the crack tip, and in the primary and secondary stages of creep at moderate distances from the tip.

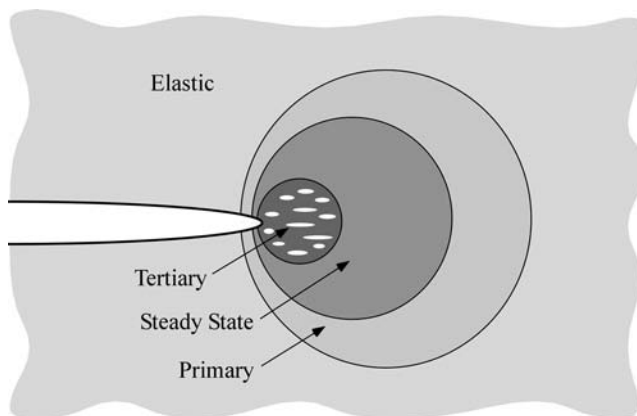


FIGURE 4.17 Creep zones at the tip of a crack.

Most analytical treatments of creep crack growth assume limiting cases, where one or more of these regimes are not present or are confined to a small portion of the component. If, for example, the component is predominantly elastic, and the creep zone is confined to a small region near the crack tip, the crack growth can be characterized by the stress-intensity factor. In the other extreme, when the component deforms globally in steady-state creep, elastic strains and tertiary creep can be disregarded. A parameter that applies to the latter case is described below, followed by a brief discussion of approaches that consider the transition from elastic to steady-state creep behavior.

4.2.1 THE C^* INTEGRAL

A formal fracture mechanics approach to creep crack growth was developed soon after the J integral was established as an elastic-plastic fracture parameter. Landes and Begley [45], Ohji et al. [46], and Nikbin et al. [47] independently proposed what became known as the C^* integral to characterize crack growth in a material undergoing steady-state creep. They applied Hoff's analogy [48], which states that if there exists a nonlinear elastic body that obeys the relationship $\epsilon_{ij} = f(\sigma_{ij})$ and a viscous body that is characterized by $\dot{\epsilon}_{ij} = f(\sigma_{ij})$, where the function of stress is the same for both, then both bodies develop identical stress distributions when the same load is applied. Hoff's analogy can be applied to steady-state creep, since the creep rate is a function only of the applied stress.

The C^* integral is defined by replacing strains with strain rates, and displacements with displacement rates in the J contour integral:

$$C^* = \int_{\Gamma} \left(\dot{w} dy - \sigma_{ij} n_j \frac{\partial \dot{u}_i}{\partial x} ds \right) \tag{4.30}$$

where \dot{w} is the stress work rate (power) density, defined as

$$\dot{w} = \int_0^{\dot{\epsilon}_{kl}} \sigma_{ij} d\dot{\epsilon}_{ij} \tag{4.31}$$

Hoff's analogy implies that the C^* integral is path independent, because J is path independent. Also, if secondary creep follows a power law:

$$\dot{\epsilon}_{ij} = A \sigma_{ij}^n \tag{4.32}$$

where A and n are material constants, then it is possible to define an HRR-type singularity for stresses and strain rates near the crack tip:

$$\sigma_{ij} = \left(\frac{C^*}{A I_n r} \right)^{\frac{1}{n+1}} \tilde{\sigma}_{ij}(n, \theta) \tag{4.33a}$$

and

$$\dot{\epsilon}_{ij} = \left(\frac{C^*}{A I_n r} \right)^{\frac{n}{n+1}} \tilde{\epsilon}_{ij}(n, \theta) \tag{4.33b}$$

where the constants I_n , $\tilde{\sigma}_{ij}$, and $\tilde{\epsilon}_{ij}$ are identical to the corresponding parameters in the HRR relationship (Equation (3.24)). Note that in the present case, n is a creep exponent rather than a strain-hardening exponent.

Just as the J integral characterizes the crack-tip fields in an elastic or elastic-plastic material, the C^* integral uniquely defines crack-tip conditions in a viscous material. Thus the time-dependent crack growth rate in a viscous material should depend only on the value of C^* . Experimental studies [45–49] have shown that creep crack growth rates correlate very well with C^* , provided steady-state creep is the dominant deformation mechanism in the specimen. Figure 4.18 shows typical creep crack growth data. Note that the crack growth rate follows a power law:

$$\dot{a} = \gamma(C^*)^m \tag{4.34}$$

where γ and m are material constants. In many materials, $m \approx n/(n + 1)$, a result that is predicted by grain boundary cavitation models [49].

Experimental measurements of C^* take advantage of analogies with the J integral. Recall that J is usually measured by invoking the energy release rate definition:

$$J = -\frac{1}{B} \left(\frac{\partial}{\partial a} \int_0^\Delta P d\Delta \right)_\Delta \tag{4.35}$$

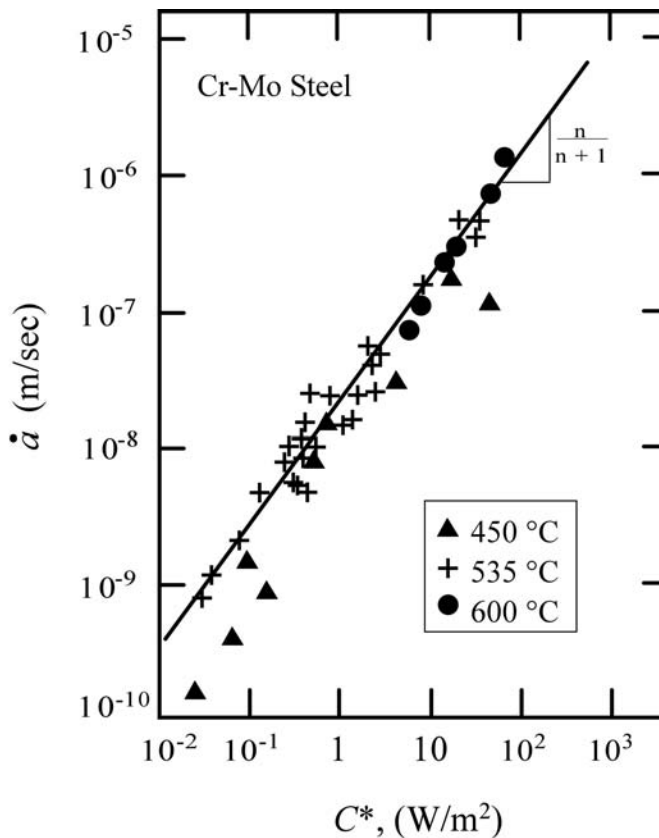


FIGURE 4.18 Creep crack growth data in a Cr-Mo Steel at three temperatures. Taken from Riedel, H., “Creep Crack Growth.” ASTM STP 1020, American Society for Testing and Materials, Philadelphia, PA, 1989, pp. 101–126.

where P is the applied load and Δ is the load-line displacement. Similarly, C^* can be defined in terms of a power release rate:

$$C^* = -\frac{1}{B} \left(\frac{\partial}{\partial a} \int_0^\Delta P d\dot{\Delta} \right)_{\dot{\Delta}} \quad (4.36)$$

The J integral can be related to the energy absorbed by a laboratory specimen, divided by the ligament area:²

$$J = \frac{\eta}{Bb} \int_0^\Delta P d\Delta \quad (4.37)$$

where η is a dimensionless constant that depends on geometry. Therefore, C^* is given by

$$C^* = \frac{\eta}{Bb} \int_0^\Delta P d\dot{\Delta} \quad (4.38)$$

For a material that creeps according to a power law (Equation (4.32)), the displacement rate is proportional to P^n , assuming global creep in the specimen. In this case, Equation (4.38) reduces to

$$C^* = \frac{n}{n+1} \frac{\eta}{Bb} P \dot{\Delta} \quad (4.39)$$

The geometry factor η has been determined for a variety of test specimens. For example, $\eta = 2.0$ for a deeply notched bend specimen (Equation (3.37) and Equation (4.6)).

4.2.2 SHORT-TIME VS. LONG-TIME BEHAVIOR

The C^* parameter applies only to crack growth in the presence of global steady-state creep. Stated another way, C^* applies to long-time behavior, as discussed below.

Consider a stationary crack in a material that is susceptible to creep deformation. If a remote load is applied to the cracked body, the material responds almost immediately with the corresponding elastic strain distribution. Assuming the loading is pure Mode I, the stresses and strains exhibit a $1/\sqrt{r}$ singularity near the crack tip and are uniquely defined by K_I . However, large-scale creep deformation does not occur immediately. Soon after the load is applied, a small creep zone, analogous to a plastic zone, forms at the crack tip. The crack-tip conditions can be characterized by K_I as long as the creep zone is embedded within the singularity dominated zone. The creep zone grows with time, eventually invalidating K_I as a crack-tip parameter. At long times, the creep zone spreads throughout the entire structure.

When the crack grows with time, the behavior of the structure depends on the crack growth rate relative to the creep rate. In brittle materials, the crack growth rate is so fast that it overtakes the creep zone; crack growth can be characterized by K_I because the creep zone at the tip of the

² The load-line displacement Δ in Equation (4.37)–(4.39) corresponds to the portion of the displacement due to the presence of the crack, as discussed in Section 3.2.5. This distinction is not necessary in Equation (4.35) and Equation (4.36), because the displacement component attributed to the uncracked configuration vanishes when differentiated with respect to a .

growing crack remains small. At the other extreme, if the crack growth is sufficiently slow that the creep zone spreads throughout the structure, C^* is the appropriate characterizing parameter.

Riedel and Rice [50] analyzed the transition from short-time elastic behavior to long-time viscous behavior. They assumed a simplified stress-strain rate law that neglects primary creep:

$$\dot{\epsilon} = \frac{\dot{\sigma}}{E} + A\sigma^n \quad (4.40)$$

for uniaxial tension. If a load is suddenly applied and then held constant, a creep zone gradually develops in an elastic singularity zone, as discussed earlier. Riedel and Rice argued that the stresses well within the creep zone can be described by

$$\sigma_{ij} = \left(\frac{C(t)}{AI_n r} \right)^{\frac{1}{n+1}} \tilde{\sigma}_{ij}(n, \theta) \quad (4.41)$$

where $C(t)$ is a parameter that characterizes the amplitude of the local stress singularity in the creep zone; $C(t)$ varies with time and is equal to C^* in the limit of long-time behavior. If the remote load is fixed, the stresses in the creep zone relax with time, as creep strain accumulates in the crack-tip region. For small-scale creep conditions, $C(t)$ decays as $1/t$ according to the following relationship:

$$C(t) = \frac{K_I^2(1-\nu^2)}{(n+1)Et} \quad (4.42)$$

The approximate size of the creep zone is given by

$$r_c(\theta, t) = \frac{1}{2\pi} \left(\frac{K_I}{E} \right)^2 \left[\frac{(n+1)AI_n E^n t}{2\pi(1-\nu^2)} \right]^{\frac{2}{n-1}} \tilde{r}_c(\theta, n) \quad (4.43)$$

At $\theta = 90^\circ$, \tilde{r}_c is a maximum and ranges from 0.2 to 0.5, depending on n . As r_c increases in size, $C(t)$ approaches the steady-state value C^* . Riedel and Rice defined a characteristic time for the transition from short-time to long-time behavior:

$$t_1 = \frac{K_I^2(1-\nu^2)}{(n+1)EC^*} \quad (4.44a)$$

or

$$t_1 = \frac{J}{(n+1)C^*} \quad (4.44b)$$

When significant crack growth occurs over time scales much less than t_1 , the behavior can be characterized by K_I , while C^* is the appropriate parameter when significant crack growth requires times $\gg t_1$. Based on a finite element analysis, Ehlers and Riedel [51] suggested the following simple formula to interpolate between small-scale creep and extensive creep (short- and long-time behavior, respectively):

$$C(t) \approx C^* \left(\frac{t_1}{t} + 1 \right) \quad (4.45)$$

Note the similarity to the transition time concept in dynamic fracture (Section 4.1.1). In both instances, a transition time characterizes the interaction between two competing phenomena.

4.2.2.1 The C_t Parameter

Unlike K_I and C^* , a direct experimental measurement of $C(t)$ under transient conditions is usually not possible. Consequently, Saxena [52] defined an alternate parameter C_t which was originally intended as an approximation of $C(t)$. The advantage of C_t is that it can be measured relatively easily.

Saxena began by separating global displacement into instantaneous elastic and time-dependent creep components:

$$\Delta = \Delta_e + \Delta_t \tag{4.46}$$

The creep displacement Δ_t increases with time as the creep zone grows. Also, if load is fixed, $\dot{\Delta}_t = \dot{\Delta}_t$. The C_t parameter is defined as the creep component of the power release rate:

$$C_t = -\frac{1}{B} \left(\frac{\partial}{\partial a} \int_0^{\Delta_t} P d\dot{\Delta}_t \right) \tag{4.47}$$

Note the similarity between Equation (4.36) and Equation (4.47).

For small-scale creep conditions, Saxena defined an effective crack length, analogous to the Irwin plastic zone correction described in Chapter 2:

$$a_{eff} = a + \beta r_c \tag{4.48}$$

where $\beta \approx \frac{1}{3}$ and r_c is defined at $\theta = 90^\circ$. The displacement due to the creep zone is given by

$$\Delta_t = \Delta - \Delta_e = P \frac{dC}{da} \beta r_c \tag{4.49}$$

where C is the elastic compliance, defined in Chapter 2. Saxena showed that the small-scale creep limit for C_t can be expressed as follows:

$$(C_t)_{ssc} = \left(\frac{f' \left(\frac{a}{W} \right)}{f \left(\frac{a}{W} \right)} \right) \frac{P \dot{\Delta}_t}{BW} \tag{4.50}$$

where $f(a/W)$ is the geometry correction factor for Mode I stress intensity (see Table 2.4):

$$f \left(\frac{a}{W} \right) = \frac{K_I B \sqrt{W}}{P}$$

and f' is the first derivative of f . Equation (4.50) predicts that $(C_t)_{ssc}$ is proportional to K_I^4 ; thus C_t does not coincide with $C(t)$ in the limit of small-scale creep (Equation (4.42)).

Saxena proposed the following interpolation between small-scale creep and extensive creep:

$$C_t = (C_t)_{ssc} \left(1 - \frac{\dot{\Delta}}{\dot{\Delta}_t} \right) + C^* \tag{4.51}$$

where C^* is determined from Equation (4.38) using the *total* displacement rate. In the limit of long-time behavior, $C^*/C_t = 1.0$, but this ratio is less than unity for small-scale creep and transient behavior.

Bassani et al. [53] applied the C_t parameter to experimental data with various C^*/C_t ratios and found that C_t characterized crack growth rates much better than C^* or K_I . They state that C_t , when defined by Equation (4.50) and Equation (4.51), characterizes experimental data better than $C(t)$, as defined by Riedel's approximation (Equation (4.45)).

Although C_t was originally intended as an approximation of $C(t)$, it has become clear that these two parameters are distinct from one another. The $C(t)$ parameter characterizes the stresses ahead of a stationary crack, while C_t is related to the rate of expansion of the creep zone. The latter quantity appears to be better suited to materials that experience relatively rapid creep crack growth. Both parameters approach C^* in the limit of steady-state creep.

4.2.2.2 Primary Creep

The analyses introduced so far do not consider primary creep. Referring to Figure 4.17, which depicts the most general case, the outer ring of the creep zone is in the primary stage of creep. Primary creep may have an appreciable effect on the crack growth behavior if the size of the primary zone is significant.

Recently, researchers have begun to develop crack growth analyses that include the effects of primary creep. One such approach [54] considers a strain-hardening model for the primary creep deformation, resulting in the following expression for total strain rate:

$$\dot{\epsilon} = \frac{\dot{\sigma}}{E} + A_1 \sigma^n + A_2 \sigma^{m(1+p)} \epsilon^{-p} \quad (4.51)$$

Riedel [54] introduced a new parameter C_h^* which is the primary creep analog to C^* . The characteristic time that defines the transition from primary to secondary creep is defined as

$$t_2 = \left(\frac{C_h^*}{(1+p)C^*} \right)^{\frac{p+1}{p}} \quad (4.52)$$

The stresses within the steady-state creep zone are still defined by Equation (4.41), but the interpolation scheme for $C(t)$ is modified when primary creep strains are present [54]:

$$C(t) \approx \left[\frac{t_1}{t} + \left(\frac{t_2}{t} \right)^{\frac{p+1}{p}} + 1 \right] C^* \quad (4.53)$$

Equation (4.53) has been applied to experimental data in a limited number of cases. This relationship appears to give a better description of experimental data than Equation (4.45), where the primary term is omitted.

Chun-Pok and McDowell [55] have incorporated the effects of primary creep into the estimation of the C_t parameter.

4.3 VISCOELASTIC FRACTURE MECHANICS

Polymeric materials have seen increasing service in structural applications in recent years. Consequently, the fracture resistance of these materials has become an important consideration. Much of the fracture mechanics methodology that was developed for metals is not directly transferable to polymers, however, because the latter behave in a viscoelastic manner.

Theoretical fracture mechanics analyses that incorporate viscoelastic material response are relatively new, and practical applications of viscoelastic fracture mechanics are rare, as of this writing. Most current applications to polymers utilize conventional, time-independent fracture mechanics methodology (see Chapter 6 and Chapter 8). Approaches that incorporate time dependence should become more widespread, however, as the methodology is developed further and is validated experimentally.

This section introduces viscoelastic fracture mechanics and outlines a number of recent advances in this area. The work of Schapery [56–61] is emphasized, because he has formulated the most complete theoretical framework, and his approach is related to the J and C^* integrals, which were introduced earlier in this text.

4.3.1 LINEAR VISCOELASTICITY

Viscoelasticity is perhaps the most general (and complex) type of time-dependent material response. From a continuum mechanics viewpoint, viscoplastic creep in metals is actually a special case of viscoelastic material behavior. While creep in metals is generally considered permanent deformation, the strains can recover with time in viscoelastic materials. In the case of polymers, time-dependent deformation and recovery is a direct result of their molecular structure, as discussed in Chapter 6.

Let us introduce the subject by considering linear viscoelastic material behavior. In this case, *linear* implies that the material meets two conditions: superposition and proportionality. The first condition requires that stresses and strains at time t be additive. For example, consider two uniaxial strains ε_1 and ε_2 , at time t , and the corresponding stresses $\sigma(\varepsilon_1)$ and $\sigma(\varepsilon_2)$. Superposition implies

$$\sigma[\varepsilon_1(t)] + \sigma[\varepsilon_2(t)] = \sigma[\varepsilon_1(t) + \varepsilon_2(t)] \quad (4.54)$$

If each stress is multiplied by a constant, the proportionality condition gives

$$\lambda_1 \sigma[\varepsilon_1(t)] + \lambda_2 \sigma[\varepsilon_2(t)] = \sigma[\lambda_1 \varepsilon_1(t) + \lambda_2 \varepsilon_2(t)] \quad (4.55)$$

If a uniaxial constant stress creep test is performed on a linear viscoelastic material, such that $\sigma = 0$ for $t < 0$ and $\sigma = \sigma_o$ for $t > 0$, the strain increases with time according to

$$\varepsilon(t) = D(t)\sigma_o \quad (4.56)$$

where $D(t)$ is the creep compliance. The loading in this case can be represented more compactly as $\sigma_o H(t)$, where $H(t)$ is the Heaviside step function, defined as

$$H(t) \equiv \begin{cases} 0 & \text{for } t < 0 \\ 1 & \text{for } t > 0 \end{cases}$$

In the case of a constant uniaxial strain, i.e., $\varepsilon = \varepsilon_o H(t)$, the stress is given by

$$\sigma(t) = E(t)\varepsilon_o \quad (4.57)$$

where $E(t)$ is the relaxation modulus. When ε_o is positive, the stress relaxes with time. Figure 4.19 schematically illustrates creep at a constant stress, and stress relaxation at a fixed strain.

When stress and strain both vary, the entire deformation history must be taken into account. The strain at time t is obtained by summing the strain increments from earlier times.

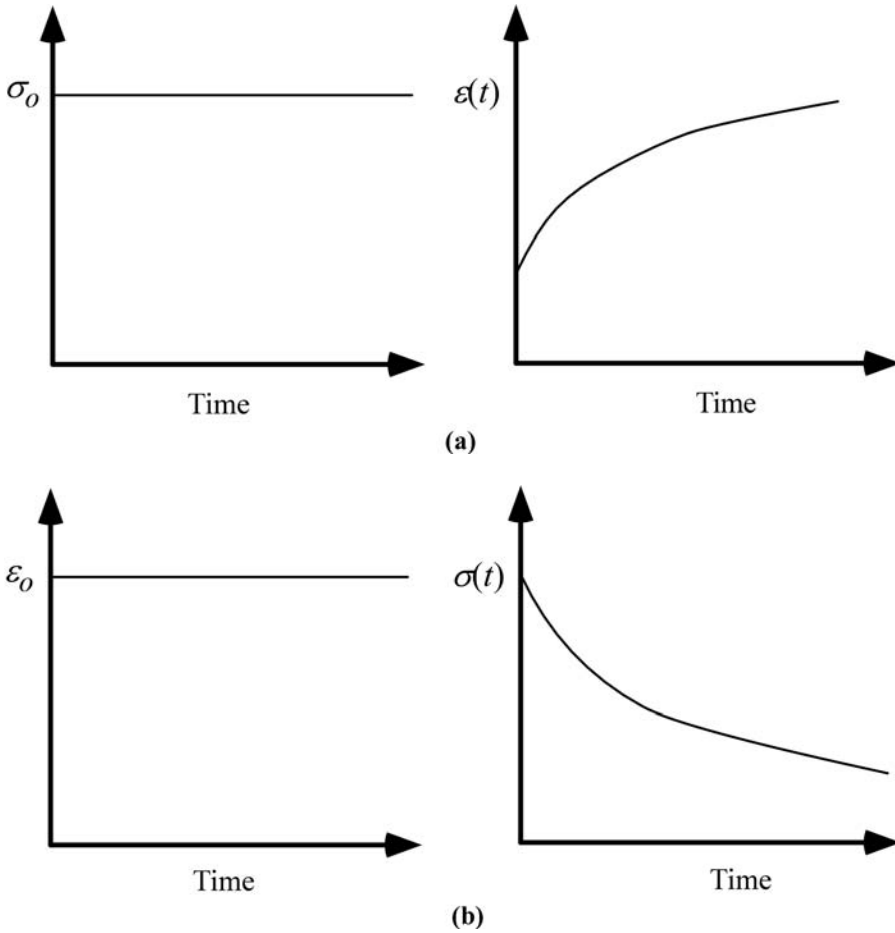


FIGURE 4.19 Schematic uniaxial viscoelastic deformation: (a) creep at a constant stress and (b) stress relaxation at a constant strain.

The incremental strain at time τ , where $0 < \tau < t$, that results from an incremental stress $d\sigma H(t - \tau)$ is given by

$$d\epsilon(\tau) = D(t - \tau)d\sigma(\tau) \tag{4.58}$$

Integrating this expression with respect to time t gives

$$\epsilon(t) = \int_0^t D(t - \tau) \frac{d\sigma(\tau)}{d\tau} d\tau \tag{4.59}$$

where it is assumed that $\epsilon = \sigma = 0$ at $t = 0$. In order to allow for a discontinuous change in stress at $t = 0$, the lower integration limit is assumed to be 0^- , an infinitesimal time before $t = 0$. Relationships such as Equation (4.59) are called *hereditary integrals* because the conditions at time t depend on prior history. The corresponding hereditary integral for stress is given by the inverse of Equation (4.59):

$$\sigma(t) = \int_0^t E(t - \tau) \frac{d\epsilon(\tau)}{d\tau} d\tau \tag{4.60}$$

By performing a Laplace transform on Equation (4.59) and Equation (4.60), it can be shown that the creep compliance and the relaxation modulus are related as follows:

$$\int_{\tau_0}^t E(t-\tau) \frac{dD(\tau-\tau_0)}{d\tau} d\tau = H(t-\tau_0) \tag{4.61}$$

For deformation in three dimensions, the generalized hereditary integral for strain is given by

$$\varepsilon_{ij}(t) = \int_0^t D_{ijkl} \left(t-\tau \frac{d\sigma_{kl}(\tau)}{d\tau} \right) d\tau \tag{4.62}$$

but symmetry considerations reduce the number of independent creep compliance constants. In the case of a linear viscoelastic isotropic material, there are two independent constants, and the mechanical behavior can be described by $E(t)$ or $D(t)$, which are uniquely related, plus $\nu_c(t)$, the Poisson's ratio for creep.

Following an approach developed by Schapery [59], it is possible to define a pseudo-elastic strain, which for uniaxial conditions is given by

$$\varepsilon^e(t) = \frac{\sigma(t)}{E_R} \tag{4.63}$$

where E_R is a reference modulus. Substituting Equation (4.63) into Equation (4.59) gives

$$\varepsilon(t) = E_R \int_0^t D(t-\tau) \frac{d\varepsilon^e(\tau)}{d\tau} d\tau \tag{4.64}$$

The pseudo-strains in three dimensions are related to the stress tensor through Hooke's law, assuming isotropic material behavior:

$$\varepsilon_{ij}^e = E_R^{-1} [(1+\nu)\sigma_{ij} - \nu\sigma_{kk}\delta_{ij}] \tag{4.65}$$

where δ_{ij} is the Kronecker delta, and the standard convention of summation on repeated indices is followed. If $\nu_c = \nu = \text{constant}$ with time, it can be shown that the three-dimensional generalization of Equation (4.64) is given by

$$\varepsilon_{ij}(t) = E_R \int_0^t D(t-\tau) \frac{d\varepsilon_{ij}^e(\tau)}{d\tau} d\tau \tag{4.66}$$

and the inverse of Equation (4.66) is as follows:

$$\varepsilon_{ij}^e(t) = E_R^{-1} \int_0^t E(t-\tau) \frac{d\varepsilon_{ij}(\tau)}{d\tau} d\tau \tag{4.67}$$

The advantage of introducing pseudo-strains is that they can be related to stresses through Hooke's law. Thus, if a linear elastic solution is known for a particular geometry, it is possible to determine the corresponding linear viscoelastic solution through a hereditary integral. Given two identical configurations, one made from a linear elastic material and the other made from a linear viscoelastic material, the stresses in both bodies must be identical, and the strains are related through

Equation (4.66) or Equation (4.67), provided both configurations are subject to the same applied loads. This is a special case of a *correspondence principle*, which is discussed in more detail below; note the similarity to Hoff's analogy for elastic and viscous materials (Section 4.2).

4.3.2 THE VISCOELASTIC J INTEGRAL

4.3.2.1 Constitutive Equations

Schapery [59] developed a generalized J integral that is applicable to a wide range of viscoelastic materials. He began by assuming a nonlinear viscoelastic constitutive equation in the form of a hereditary integral:

$$\varepsilon_{ij}(t) = E_R \int_0^t D(t-\tau, t) \frac{\partial \varepsilon_{ij}^e(\tau)}{\partial \tau} d\tau \quad (4.68)$$

where the lower integration limit is taken as 0^- . The pseudo-elastic strain ε_{ij}^e is related to stress through a linear or nonlinear elastic constitutive law. The similarity between Equation (4.66) and Equation (4.68) is obvious, but the latter relationship also applies to certain types of nonlinear viscoelastic behavior. The creep compliance $D(t)$ has a somewhat different interpretation for the nonlinear case.

The pseudo-strain tensor and reference modulus in Equation (4.68) are analogous to the linear case. In the previous section, these quantities were introduced to relate a linear viscoelastic problem to a reference elastic problem. This idea is generalized in the present case, where the nonlinear viscoelastic behavior is related to a reference nonlinear elastic problem through a correspondence principle, as discussed below.

The inverse of Equation (4.68) is given by

$$\varepsilon_{ij}^e(t) = E_R^{-1} \int_0^t E(t-\tau, t) \frac{\partial \varepsilon_{ij}(\tau)}{\partial \tau} d\tau \quad (4.69)$$

Since hereditary integrals of the form of Equation (4.68) and Equation (4.69) are used extensively in the remainder of this discussion, it is convenient to introduce an abbreviated notation:

$$\{Ddf\} \equiv E_R \int_0^t D(t-\tau, t) \frac{\partial f}{\partial \tau} d\tau \quad (4.70a)$$

and

$$\{Edf\} \equiv E_R^{-1} \int_0^t E(t-\tau, t) \frac{\partial f}{\partial \tau} d\tau \quad (4.70b)$$

where f is a function of time. In each case, it is assumed that integration begins at 0^- . Thus Equation (4.68) and Equation (4.69) become, respectively,

$$\varepsilon_{ij}(t) = \{Dd\varepsilon_{ij}^e\} \quad \text{and} \quad \varepsilon_{ij}^e = \{Ed\varepsilon_{ij}\}$$

4.3.2.2 Correspondence Principle

Consider two bodies with the same instantaneous geometry, where one material is elastic and the other is viscoelastic and is described by Equation (4.68). Assume that at time t , a surface traction $T_i = \sigma_{ij}n_j$ is applied to both configurations along the outer boundaries. If the stresses

and strains in the elastic body are σ_{ij}^e and ϵ_{ij}^e , respectively, while the corresponding quantities in the viscoelastic body are σ_{ij} and ϵ_{ij} , the stresses, strains, and displacements are related as follows [59]:

$$\sigma_{ij} = \sigma_{ij}^e, \quad \epsilon_{ij} = \{Dd\epsilon_{ij}^e\}, \quad u_i = \{Ddu_i^e\} \tag{4.71}$$

Equation (4.71) defines a correspondence principle, introduced by Schapery [59], which allows the solution to a viscoelastic problem to be inferred from a reference elastic solution. This correspondence principle stems from the fact that the stresses in both bodies must satisfy equilibrium, and the strains must satisfy compatibility requirements in both cases. Also, the stresses are equal on the boundaries by definition:

$$T_i = \sigma_{ij}n_j = \sigma_{ij}^en_j$$

Schapery [59] gives a rigorous proof of Equation (4.71) for viscoelastic materials that satisfy Equation (4.68).

Applications of correspondence principles in viscoelasticity, where the viscoelastic solution is related to a corresponding elastic solution, usually involve performing a Laplace transform on a hereditary integral in the form of Equation (4.62), which contains actual stresses and strains. The introduction of pseudo-quantities makes the connection between viscoelastic and elastic solutions more straightforward.

4.3.2.3 Generalized *J* Integral

The correspondence principle in Equation (4.71) makes it possible to define a generalized time-dependent *J* integral by forming an analogy with the nonlinear elastic case:

$$J_v = \int_{\Gamma} \left(w^e dy - \sigma_{ij}n_j \frac{\partial u_i^e}{\partial x} ds \right) \tag{4.72}$$

where w^e is the pseudo-strain energy density:

$$w^e = \int \sigma_{ij}^e d\epsilon_{ij}^e \tag{4.73}$$

The stresses in Equation (4.72) are the actual values in the body, but the strains and displacements are pseudo-elastic values. The actual strains and displacements are given by Equation (4.71). Conversely, if ϵ_{ij} and u_i are known, J_v can be determined by computing pseudo-values, which are inserted into Equation (4.73). The pseudo-strains and displacements are given by

$$\epsilon_{ij}^e = \{Ed\epsilon_{ij}\} \quad \text{and} \quad u_i^e = \{Edu_i\} \tag{4.74}$$

Consider a simple example, where the material exhibits steady-state creep at $t > t_0$. The hereditary integrals for strain and displacement reduce to

$$\epsilon_{ij}^e = \dot{\epsilon}_{ij} \quad \text{and} \quad u_i^e = \dot{u}_i$$

By inserting the above results into Equation (4.73), we see that $J_v = C^*$. Thus C^* is a special case of J_v . The latter parameter is capable of taking account of a wide range of time-dependent material behavior, and includes viscous creep as a special case.

Near the tip of the crack, the stresses and pseudo-strains are characterized by J_v through an HRR-type relationship in the form of Equation (4.33). The viscoelastic J can also be determined through a pseudo-energy release rate:

$$J_v = -\frac{1}{B} \left(\frac{\partial}{\partial a} \int_0^{\Delta^e} P d\Delta^e \right)_{\Delta^e} \tag{4.75}$$

where Δ^e is the pseudo-displacement in the loading direction, which is related to the actual displacement by

$$\Delta = \{Dd\Delta^e\} \tag{4.76}$$

Finally, for Mode I loading of a linear viscoelastic material in plane strain, J_v is related to the stress-intensity factor as follows:

$$J_v = \frac{K_I^2(1-\nu^2)}{E_R} \tag{4.77}$$

The stress-intensity factor is related to specimen geometry, applied loads, and crack dimensions through the standard equations outlined in Chapter 2.

4.3.2.4 Crack Initiation and Growth

When characterizing crack initiation and growth, it is useful to relate J_v to physical parameters such as CTOD and fracture work, which can be used as local failure criteria. Schapery [59] derived simplified relationships between these parameters by assuming a strip-yield-type failure zone ahead of the crack tip, where a closure stress σ_m acts over ρ , as illustrated in Figure 4.20. While the

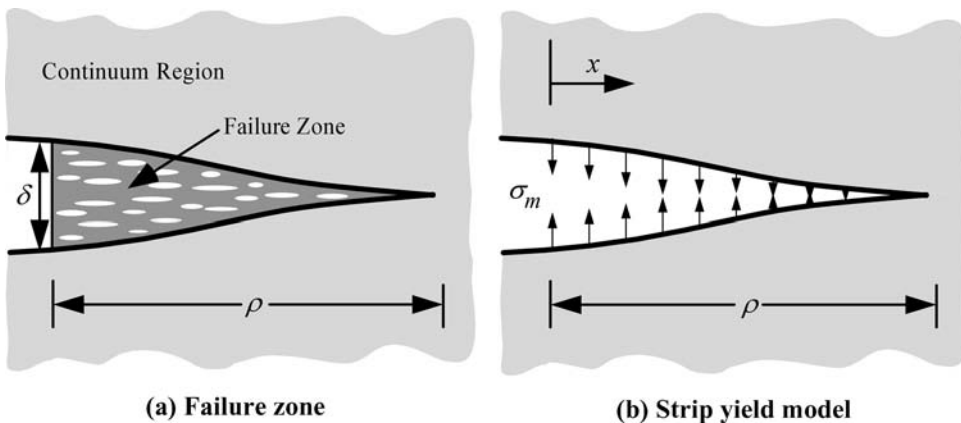


FIGURE 4.20 Failure zone at the crack tip in a viscoelastic material. This zone is modeled by surface tractions within $0 < x < \rho$.

material in the failure zone may be severely damaged and contain voids and other discontinuities, it is assumed that the surrounding material can be treated as a continuum. If σ_m does not vary with x , applying Equation (3.44) gives

$$J_v = \sigma_m \delta^e \tag{4.78}$$

where δ^e is the pseudo-crack-tip-opening displacement, which is related to the actual CTOD through a hereditary integral of the form of Equation (4.77). Thus the CTOD is given by

$$\delta = \{Dd(J_v/\sigma_m)\} \tag{4.79}$$

Although σ_m was assumed to be independent of x at time t , Equation (4.79) permits σ_m to vary with time. The CTOD can be utilized as a local failure criterion: If crack initiation occurs at δ_i , the J_v at initiation can be inferred from Equation (4.79). If δ_i is assumed to be constant, the critical J_v would, in general, depend on the strain rate. A more general version of Equation (4.79) can be derived by allowing σ_m to vary with x .

An alternative local failure criterion is the fracture work w_f . Equating the work input to the crack tip to the energy required to advance the crack tip by da results in the following energy balance at initiation:

$$\int_0^{\delta_i} \sigma_m d\delta = 2w_f \tag{4.80}$$

assuming unit thickness and Mode I loading. This energy balance can also be written in terms of a time integral:

$$\int_0^{\tau_i} \sigma_m \frac{\partial \delta}{\partial t} dt = 2w_f \tag{4.81}$$

Inserting Equation (4.79) into Equation (4.81) gives

$$\int_0^{\tau_i} \sigma_m \frac{\partial \{Dd(J_v/\sigma_m)\}}{\partial t} dt = 2w_f \tag{4.82}$$

If σ_m is independent of time, it cancels out of Equation (4.82), which then simplifies to

$$E_R \int_0^{\tau_i} D(t_i - \tau, t_i) \frac{\partial J_v}{\partial \tau} d\tau = 2w_f \tag{4.83}$$

For an elastic material, $D = E_R^{-1}$ and $J_v = 2w_f$. If the failure zone is viscoelastic and the surrounding continuum is elastic, J_v may vary with time. If the surrounding continuum is viscous, $D = (t - \tau)/(t_v E_R)$, where t_v is a constant with units of time. Inserting this latter result into Equation (4.83) and integrating by parts gives

$$t_v^{-1} \int_0^{t_i} J_v dt = 2w_f \tag{4.84}$$

4.3.3 TRANSITION FROM LINEAR TO NONLINEAR BEHAVIOR

Typical polymers are linear viscoelastic at low stresses and nonlinear at high stresses. A specimen that contains a crack may have a zone of nonlinearity at the crack tip, analogous to a plastic zone, which is surrounded by linear viscoelastic material. The approach described in the previous section applies only when one type of behavior (linear or nonlinear) dominates.

Schapery [61] has modified the J_v concept to cover the transition from small-stress to large-stress behavior. He introduced a modified constitutive equation, where the strain is given by the sum of two hereditary integrals: one corresponding to linear viscoelastic strains and the other describing nonlinear strains. For the latter term, he assumed power-law viscoelasticity. For the case of uniaxial constant tensile stress σ_o the creep strain in this modified model is given by

$$\varepsilon(t) = E_R D(t) \left(\frac{\sigma_o}{\sigma_{ref}} \right)^n + D_L(t) \sigma_o \quad (4.85)$$

where D and D_L are the nonlinear and linear creep compliance, respectively, and σ_{ref} is a reference stress.

At low stresses and short times, the second term in Equation (4.85) dominates, while the nonlinear term dominates at high stresses or long times. In the case of a viscoelastic body with a stationary crack at a fixed load, the nonlinear zone is initially small but normally increases with time, until the behavior is predominantly nonlinear. Thus there is a direct analogy between the present case and the transition from elastic to viscous behavior described in Section 4.2.

Close to the crack tip, but outside of the failure zone, the stresses are related to a pseudo-strain through a power law:

$$\varepsilon^e = \left(\frac{\sigma_o}{\sigma_{ref}} \right)^n \quad (4.86)$$

In the region dominated by Equation (4.86), the stresses are characterized by J_v , regardless of whether the global behavior is linear or nonlinear:

$$\sigma_{ij} = \sigma_{ref} \left(\frac{J_v}{\sigma_{ref} J_n r} \right)^{\frac{1}{n+1}} \tilde{\sigma}_{ij}(n, \theta) \quad (4.87)$$

If the global behavior is linear, there is a second singularity further away from the crack tip:

$$\sigma_{ij} = \frac{K_I}{\sqrt{2\pi r}} f_{ij}(\theta) \quad (4.88)$$

Let us define a pseudo-strain tensor that, when inserted into the path-independent integral of Equation (4.72), yields a value J_L . Also suppose that this pseudo-strain tensor is related to the stress tensor by means of linear and power-law pseudo-complementary strain energy density functions (w_{cl} and w_{cn} , respectively):

$$\varepsilon_{ij}^{eL} = \frac{\partial}{\partial \sigma_{ij}} (f w_{cn} + w_{cl}) \quad (4.89)$$

where $f(t)$ is an as yet unspecified aging function, and the complementary strain energy density is defined by

$$w_c = \int \varepsilon_{ij}^{eL} d\sigma_{ij}$$

For uniaxial deformation, Equation (4.89) reduces to

$$\varepsilon^{eL} = f \left(\frac{\sigma}{\sigma_{ref}} \right)^n + \frac{\sigma}{E_R} \tag{4.90}$$

Comparing Equation (4.85) and Equation (4.90), it can be seen that

$$f = \frac{D(t)}{D_L(t)} \quad \text{if} \quad \varepsilon^{eL} \equiv \frac{\varepsilon(t)}{E_R D_L(t)} \quad \text{for constant stress creep.}$$

The latter relationship for pseudo-strain agrees with the conventional definition in the limit of linear behavior.

Let us now consider the case where the inner and outer singularities, Equation (4.87) and Equation (4.88), exist simultaneously. For the outer singularity, the second term in Equation (4.90) dominates, the stresses are given by Equation (4.88), and J_L is related to K_I as follows:

$$J_L = \frac{K_I^2(1-\nu^2)}{E_R} \tag{4.91}$$

Closer to the crack tip, the stresses are characterized by J_v through Equation (4.87), but J_L is not necessarily equal to J_v , because f appears in the first term of the modified constitutive relationship (Equation (4.90)), but not in Equation (4.86). These two definitions of J coincide if σ_{ref} in Equation (4.90) is replaced with $\sigma_{ref} f^{1/n}$. Thus, the near-tip singularity in terms of J_L is given by

$$\sigma_{ij} = \sigma_{ref} \left(\frac{J_L}{f \sigma_{ref} I_n r} \right)^{\frac{1}{n+1}} \tilde{\sigma}_{ij}(n, \theta) \tag{4.92}$$

therefore,

$$J_v = \frac{J_L}{f} \tag{4.93}$$

Schapery showed that $f = 1$ in the limit of purely linear behavior; thus J_L is the limiting value of J_v when the nonlinear zone is negligible. The function f is indicative of the extent of nonlinearity. In most cases, f increases with time, until J_v reaches J_n , the limiting value when the specimen is dominated by nonlinear viscoelasticity. Schapery also confirmed that

$$f = \frac{D(t)}{D_L(t)} \tag{4.94}$$

for small-scale nonlinearity. Equation (4.93) and Equation (4.94) provide a reasonable description of the transition to nonlinear behavior. Schapery defined a transition time by setting $J_v = J_n$ in Equation (4.93):

$$J_n = \frac{J_L}{f(t_\tau)} \quad (4.95a)$$

or

$$t_\tau = f^{-1}\left(\frac{J_L}{J_n}\right) \quad (4.95b)$$

For the special case of linear behavior followed by viscous creep, Equation (4.95b) becomes

$$t_\tau = \frac{J_L}{(n+1)C^*} \quad (4.96)$$

which is identical to the transition time defined by Riedel and Rice [50].

APPENDIX 4: DYNAMIC FRACTURE ANALYSIS

A4.1 ELASTODYNAMIC CRACK TIP FIELDS

Rice [31], Sih [35], and Irwin [62] each derived expressions for the stresses ahead of a crack propagating at a constant speed. They found that the moving crack retained the $1/\sqrt{r}$ singularity, but that the angular dependence of the stresses, strains, and displacements depends on crack speed. Freund and Clifton [32] and Nilsson [33] later showed that the solution for a constant speed crack was valid in general; the near-tip quantities depend only on instantaneous crack speed. The following derivation presents the more general case, where the crack speed is allowed to vary.

For dynamic problems, the equations of equilibrium are replaced by the equations of motion, which, in the absence of body forces, are given by

$$\frac{\partial \sigma_{ji}}{\partial x_j} = \rho \ddot{u}_i \quad (A4.1)$$

where x_j denotes the orthogonal coordinates and each dot indicates a time derivative. For quasistatic problems, the term on the right side of Equation (A4.1) vanishes. For a linear elastic material, it is possible to write the equations of motion in terms of displacements and elastic constants by invoking the strain-displacement and stress-strain relationships:

$$\mu \frac{\partial^2 u_i}{\partial x_j^2} + (\lambda + \mu) \frac{\partial^2 u_j}{\partial x_i \partial x_j} = \rho \ddot{u}_i \quad (A4.2)$$

where μ and λ are the Lamé constants; μ is the shear modulus and

$$\lambda = \frac{2\mu\nu}{1-2\nu}$$

UNIT IV - DETERMINATION OF FRACTURE TOUGHNESS VALUES

1. Introduction

Ships, aircraft and rockets are extremely complex engineering systems with many thousands of components. In the construction of such systems it is impossible to completely avoid the presence of flaws such as cracks. Understanding the strength of materials in the presence of cracks is thus key to developing reliable aerospace and ocean engineering hardware. This experiment is designed to illustrate how strength in the presence of cracks - termed Fracture Toughness - is characterized and measured. You will get to measure the fracture toughness of aluminum - the dominant material used to build aircraft and spacecraft.

Stress around a crack

Consider the idealized situation shown in figure 1. This shows a uniform material of infinite extent that contains a semi-infinite horizontal crack coincident with the negative x axis. The crack is being pulled apart by a stress acting in the y direction σ_y that far away from the crack is uniform throughout the material. The stress concentration in the vicinity of the crack may be determined analytically if the crack tip is assumed to be sharp and the material is allowed to deform only in a linear elastic fashion. Such an analysis shows that, along the positive x axis, thus the stress increases to infinity at the crack tip. Note that the overall magnitude of the stress field around the crack is controlled by the parameter K, called the stress intensity. In this idealized situation, K is proportional to the uniform tension being applied to the material. This type of an analysis is an example of Linear Elastic Fracture Mechanics, or LEFM.

The real situation is of course more complicated. Consider the cracked material specimen in figure 2. Immediately surrounding the crack the large stresses predicted by LEFM and the above equation are not realized because the material does not behave in a linear elastic fashion here. In a metal, plastic yielding occurs to relieve and redistribute the stresses. In other materials, such as polymers or ceramics, different types of deformation, such as crazing or micro-cracking, may occur. The above equation is also unrealistic far from the crack where the shape of the specimen and the loading conditions determine the stress field. In between these regions, however, is a region where the crack dominates the stress field and the material deforms elastically. This is called the region of K dominance. Equation (1) is valid here. Fortunately, as long as the plastic zone remains small compared

to the specimen size, the region of K dominance controls the behavior of the crack. This means, for example, that we can use the stress intensity K to characterize the strength of the stress field surrounding the crack.

Fracture and fracture toughness

Suppose the load on the specimen in figure 2 is increased until it fractures, i.e. the crack grows. The resistance to fracture may be characterized by the stress intensity at fracture K_c , called the fracture toughness. The fracture toughness and the manner in which the crack grows is heavily dependent upon the material thickness.

Consider a specimen having a thickness t that is small compared to the diameter of the plastic zone r_o , figure 3a. As the crack is pulled apart the plastic zone will undergo Poisson contraction, relieving stresses s_z acting through the sample in the z direction. We call this situation plane stress because stresses are only acting in the x - y plane. With s_y large and s_z near zero the shear stress on the 45° plane between the y and z axes is at a maximum. The crack therefore tends to orient itself along this plane as it grows. This type of crack growth is usually stable and gradual and is characterized as tearing.

Now consider a specimen having a thickness t that is large compared to r_o , figure 3b. As the crack is pulled apart the material above and below the plastic zone prevents Poisson contraction from occurring throughout most of the sample. This sets up large s_z stresses in the plastic zone. We call this situation plane strain because material is straining only in the x - y plane. With s_z comparable to s_y , the shear stresses are small so the crack tends to orient itself in a plane perpendicular to s_y as it grows. This type of growth is usually unstable and is characterized as cleavage. Note that even with a thick sample there will be a thin regions close to its surfaces where Poisson contraction will take place and failure on 45° planes will occur.

Thicknesses between those that result in plane strain or plane stress are termed mixed, with plane strain occurring in the interior and plane stress some significant distance from the surface.

Because the Poisson contraction in a thin specimen relieves some of the stress, the fracture toughness of such a sample is relatively high. As the sample thickness increases and the form of the stress distribution changes the fracture toughness falls, asymptoting to a constant value for plane strain. Because of its independence of sample thickness this asymptote, termed the plane strain fracture toughness K_{Ic} , is considered a material property.

2. Objective and Approach

The objective of this experiment is to determine the plane-strain fracture toughness of 7075-T651 aluminum. The fracture toughness testing procedures specified in ASTM Standard No. E399 will be used. Three compact specimens (see figure 4) of nominal thickness 1/8", 1/4" and 3/4" will be tested. Each sample contains a notch, or 'machined crack'. At the tip of the notch a true crack has been produced by repeatedly loading (fatiguing) the specimen.

To determine their fracture toughness each of the samples will be pulled apart by applying load to a pair of dowel pins mounted through the holes in each sample. The load on the sample P vs. the opening of the crack (the displacement v) will be recorded. These data, plus the sample dimensions will then be used to

Identify the load at fracture

- Determine the stress intensity at fracture and thus the fracture toughness
- Determine whether the sample was in plane stress, plane strain or a mixed state.
- Estimate the size of the plastic zone

3. Apparatus

To load the sample an Instron 4204 Universal Testing Machine will be used, connected to a computer running a Labview program. The computer is used to log the test data, but it doesn't control the testing machine. Control of the machine is through control pad on the right of the test assembly, see the inventory photos. The machine has a crosshead - a horizontal bar - that can be accurately traversed up and down by means of two large jack screws. Specimens are tested by attaching them between the crosshead and the stationary base of the machine and then traversing the crosshead up to place the sample under increasing load. The load on the sample is recorded by a piezo-electric load cell mounted between the sample and the crosshead. The range of the load cell output and its calibration are provided internally to the computer program. You can assume that the uncertainty in the indicated load is the same as the uncertainty in its offset, which you can judge by examining the typical indicated load on the sample when no force is being applied.

The testing machine is a potentially dangerous device and should be treated with great respect. A specially trained operator will be on hand (either your TA or a faculty member) to run the machine and give you safety advice. There is an emergency stop button. If you are not told, ask where it is. Do not touch any other controls on the machine without express instructions from the operator.

To measure the opening of the crack an MTS Extensometer is used. Be sure to write down the model number during the test. The extensometer has two jaws that mount to the side of the specimen on either side of the machine crack opening. The extensometer is operated by the same controller that runs the testing machine and its output is fed to the computer. You can assume that the uncertainty in the indicated displacement is the same as the uncertainty in its offset, which you will be able to judge from the raw load vs. displacement plots provided by the computer and/or by examining the typical displacement indicated when no force is being applied.

You will be given specific instructions on how to use the computer and software at the time of the experiment. Don't forget to make a complete list of the apparatus and instrumentation you are using ready for your report.

4. Procedure

Unlike the other experiments in AOE 3054 this one has a defined procedure. This is because of the importance (to safety) of using the testing machine correctly and the difficulty of preparing good samples (limiting each lab group to 3). Ironically this makes it all the more important that you cast a critical eye on the procedure, apparatus and instrumentation you are given. It is all too easy with a set procedure to assume that all the errors have been characterized and sorted out already (they haven't). Therefore preparation of a detailed electronic lab book will be a key component of performing an effective experiment, from deciding (as a group) what the objectives of the lab really are, to recording dimensions and characteristics you are maybe not asked for, to documenting the apparatus and its flaws through good digital photography. In addition to the apparatus described above you will have at your disposal the (now usual) camera and extra measuring instruments. As always objective observation, as opposed to "matching the theory" is what is being asked.

This entire section should be read before embarking on the experiment. Copy a blank version of table 1 to your log book in advance of the lab.

Determining the sample dimensions (see figure 4)

Measure the half height h and width (to hole centers) w of each of your samples using the caliper provided. Measure the thickness t of each sample using the micrometer. The length of the initial crack a_i , measured from the hole centers will also be needed. However, it is unlikely that this will be clearly visible until you can examine the fracture surfaces after the sample is broken. A close up photograph and notes on any sample flaws might make good additions to the logbook. Estimate primary uncertainties in these measurements.

Preparing the sample for test

Before testing the specimen it is necessary to attach the extensometer using rubber bands. The jaws of the extensometer rest in notches cut into the side of the sample (see figure 4). A small pin holds the jaws fixed while the extensometer is not in use. Attaching the extensometer is an awkward operation at best. Have your TA explain how to do it. Photo?

Mounting the specimen in the testing machine

Load is applied to the specimen through two half-inch diameter dowel pins. The pins pass through the holes in the specimen and matching holes in two clevis grips. Three pairs of clevis grips (with 1/8", 1/4" and 3/4" slots) are available. Select the pair of grips that match the specimen under test. Mount one to the base of the testing machine and one to the crosshead using the dowel pins provided. If necessary get the operator to move the crosshead up to give you enough space. Make sure that the flat side of both grips face to the left. Place the specimen in the slot in the lower grip with the extensometer on the left and secure it with a dowel pin. (Note that the dowel pin should be a snug fit, but you should be able to push it in by hand. Don't be tempted to hammer the pin in or you may never get it out). Have the operator lower the crosshead slowly until the holes in the sample and upper grip line up accurately enough to push a dowel pin through them. Are you really happy with how the sample sits in the jaws, how well the extensometer sits in the grooves? Estimate the primary uncertainty in the load by looking at the load with no force being applied. Estimate the primary uncertainty in displacement by looking at the fluctuations in indicated displacement as the sample sits there (the displacement will be zeroed before the test, and so only the perturbations from that zero will be visible).

Running the test

Remove the pin holding the extensometer jaws. Set the computer program ready to take data. Ask the operator to begin the test. He/she will set the Testing Machine controller to raise the crosshead at a speed of 0.05 inches per minute. As the test begins watch the drawing of the load/displacement diagram. Initially it should appear as a straight diagonal line showing the initial elastic deformation of the specimen. If you don't see this, alert the operator so that the test may be halted and the problem diagnosed before the sample is destroyed. Record all that happens, it may be a factor in the results you get.

As the load on the sample increases, you will begin to see its surface dimple around the crack (photo?). This dimpling is produced by Poisson contraction of the material in the plastic zone. As the sample begins to fracture different things will happen depending on its thickness (see 'Identifying the load at fracture' below). The sample may fail suddenly, or it may tear. In the latter case you may hear a

popping sound. This is the sound of the crack intermittently growing. The test continues until the extensometer has reached the limit of its range. At this time the extensometer is removed and the crosshead is raised to completely separate the two halves of the sample. Remove the remains of the sample from the testing machine ready for the data analysis, and save and transfer your load and displacement data so you can plot your P-v diagram in the logbook.

5. Data Analysis

Record your analysis in the lab book in a programmed version of table 1

(a) Examination of the specimen

Look over the fracture surfaces. The initial crack should be fairly obvious. Measure its average length a_i , allowing for the 0.9" distance from the end of the machine crack to the hole centers, noting particularly if it is not uniform through the specimen thickness. Look at and photograph (in plan view and cross section) the fracture itself. How much of the fracture occurs on a 45° plane? Estimate primary uncertainties in this measurement.

(b) Identifying the load at fracture

Import your load and displacement data into your logbook. Plot the P-v diagram and compare it with the samples shown in figure 5 . Initially the P-v diagram is linear because the sample deforms elastically. You will likely have to shift the origin of the plot so it lines up with this linear region (this is easily done in Excel by subtracting or adding a constant to the displacement values). How accurately can you determine the origin of the load and displacement? Use this information to modify your estimates of primary uncertainty in these. At fracture the crack will grow changing the sample stiffness and causing the P-v diagram to depart from a straight line. How this departure occurs depends on how the sample fractures. If cleavage is dominant then there will be a sharp break in the P-v diagram at fracture (figure 5 , type III). If tearing is dominant (figure 5 , type I) then the P-v diagram will become curved as fracture begins. A mixture of fracture mechanisms will produce a smooth curve punctuated by discontinuities of unstable crack growth (figure 5 , type II). These discontinuities are called 'pop in' since they produce the audible popping sound.

With such a variety of behavior, a consistent definition of the load at fracture P_Q is needed. Figure 5 illustrates this. A line is drawn from the origin with a slope (m_5) equal to 95% of the slope (m_t) of the initial linear portion of the P-v curve. The load at fracture is then taken as the maximum load supported by the sample in advance of the point where OB intersects the P-v curve. Obviously you need to think about, and quantify (in the logbook) the uncertainty in getting P_Q as this may be a major factor in your stress intensity uncertainty. Note that it is easiest to construct this 95% slope line using the drawing tools

in Excel or PowerPoint: Draw a line over your chart equal to the slope of the initial linear portion. Double-click on the line, select the 'Size' tab, and set the height scaling to 95%. Close the dialog and move the line so it once more cuts the origin of the P-v curve.

(c) Determining the stress intensity at fracture K_Q

The relationship between the stress intensity and the load applied to the sample is not a simple one since it depends on the form of the stress field far from the crack where the shape of the sample and its precise loading conditions are important. To take these into account it is necessary to perform a finite element computation, using the theory of elasticity, of the stress field in the sample. Such a computation has already been performed for the compact specimen geometry used in the present experiment. The following function is a curve fit to the results of this computation

where $a = a_i/w$. Note that this is an empirical form of equation 1 with x replaced by w and the stress replaced by PQ/tw . The calculator below computes $f(a)$, the part of equation 2 following the first parenthesis that is only a function of a . Input $a = 0.5$, press $=$, read off $f =$

(d) Determining whether sample was in plane stress or plane strain

The relationships listed in section (d) of table 1, from ASTM Standard No. E399, are used to determine whether the sample was in plane stress or plane strain. Specifically, if both conditions (on K_Q and PQ) are met then the sample was in plane strain, otherwise it was in plane stress. Note that σ_y is the yield strength of the sample material (79.1ksi), h , t and w are the sample dimensions. See if the answers you get agree with your own judgments based upon how the sample failed. Would changes to the various parameters within their uncertainty influence the conclusions here? figure this out as a group.

(e) Determining whether the plastic zone size and final results

The relationships listed in section (e) of table 1 (also from ASTM Standard No. E399) are used to determine the size of the plastic zone. As noted above, the plastic zone must be small compared to the sample size for the LEFM used to generate equation (2) to be valid. How do the results you get here compare with your impressions of the dimpling during the test? If LEFM is valid, interpret your value of K_Q as K_c or K_{Ic} . Try to estimate their uncertainties.

6. Recommended Report Format

Traditionally, test reports are as brief as possible (while being complete). It is expected that, by this stage in the course, you will have a good feel for the correct report format so no specific help is given here. However, please note that your report must include, at least;

Descriptions (in the introduction) of what fracture toughness is (as distinct from yield strength and fatigue failure); what stress intensity K is, and how it is related to stress; what K_{Ic} is; what the plastic zone is; conditions on the plastic zone for LEFM to be valid; what plane stress and plane strain are and the kinds of fracture seen under these conditions; what K_{Ic} is.

Each P-v diagram, properly labeled and plotted, according to the requirements set in appendix 1.

Discussion of the first 'pop-in' in each P-v diagram. Comment on whether the first 'pop-in' would be a reliable method of finding the the load at the beginning of crack growth? Why? Why not?

- The variation in fracture toughness with specimen thickness, correctly plotted and labeled. Discussion of the trend with thickness, with fracture mode with P-v behavior, and evidence that the values are asymptoting to K_{Ic} as the thickness increases.
- Labeled photos showing the form of the fracture surfaces revealed in the photos and discussion of whether they are consistent with the P-v behavior in each case and with the plane stress or plane strain determination.
- Discussion of how the computed plastic zone sizes compare with those suggested by extent of dimpling on the sample surfaces.

K-R CURVE TESTING

As discussed in the previous section, materials that fail by microvoid coalescence usually exhibit a rising R curve. The ASTM E 399 test method measures a single point on the R curve. This method contains an inherent size dependence on apparent toughness because the point on the R curve at which K_Q is defined is a function of the ligament length, as Figure 7.17 illustrates. An alternative to measuring a single toughness value is determining the entire R curve for materials that exhibit ductile crack extension. The ASTM Standard E 561 [14] outlines a procedure for determining K vs. crack growth curves in such materials. Unlike ASTM E 399, the K-R standard does not contain a minimum thickness requirement, and thus can be applied to thin sheets. This standard, however, is appropriate only when the plastic zone is small compared to the in-plane dimensions of the test specimen. This test method is often applied to high-strength sheet materials. As Figure 7.15 illustrates, thin sheets generally have a steeper R curve than thick sections because the slant fracture morphology dominates in the former. There is a common misconception about the effect of section thickness on the shape of the R curve. A number of published articles and textbooks imply that thick sections, corresponding to so-called plane strain fracture, exhibit a single value of fracture toughness (K_{Ic}), while the same material in a thin section displays a rising R curve. The latter is often mistakenly referred to as “plane stress fracture.” (Refer to Section 2.10 for a detailed discussion of the fallacies of the traditional

“plane stress” and “plane strain” descriptions of crack-tip conditions.) The section thickness has an effect on the crack-tip stress state and the fracture morphology, which in turn affects the slope of the R curve (Figure 7.15). However, a material that fails by microvoid coalescence usually has a rising R curve even for flat fracture under predominately plane strain conditions. The only instance where a thin section might exhibit a rising R curve while a thick section of the same material has a flat R curve (and a singlevalued toughness) is where the difference in crack-tip triaxiality causes a fracture mode change from ductile tearing to cleavage in thin and thick sections, respectively. Figure 7.19 illustrates a typical K-R curve in a predominantly linear elastic material. The R curve is initially very steep, as little or no crack growth occurs with increasing KI. As the crack begins to grow, K increases with the crack growth until a steady state is reached, where the R curve becomes flat (see Section 3.5 and Appendix 3.5). It is possible to define a critical stress intensity K_c where the driving force is tangent to the R curve. This instability point is not a material property, however, because the point of tangency depends on the shape of the driving force curve, which is governed by the size and geometry of the cracked body. In a laboratory specimen under load control, for example, K_c would correspond to P_{max} in a Type I load-displacement curve (Figure 7.13). Such a K_c value would exhibit a size dependence similar to that observed for KQ based on a 2% crack growth criterion, as Figure 7.17 illustrates. Consequently, K_c values obtained from laboratory specimens are not usually transferable to structures.

J TESTING OF METALS

The current ASTM standard that covers J-integral testing is E 1820 [4]. This standard is actually a generalized fracture toughness standard, as it also covers K_{Ic} and CTOD tests. The British Standard BS 7448: Part 1 [10] is equivalent in scope to ASTM E 1820. ASTM E 1820 has two alternative methods for J tests: the basic procedure and the resistance curve procedure. The basic procedure entails monotonically loading the specimen to failure or to a particular displacement, depending on the material behavior. The resistance curve procedure requires that the crack growth be monitored during the test. The J integral is calculated incrementally in the resistance curve procedure. The basic procedure can be used to measure J at fracture instability or near the onset of ductile crack extension. The latter toughness value is designated by the symbol J_{Ic} .

J-R CURVE TESTING

The resistance curve test method in ASTM E 1820 requires that crack growth be monitored throughout the test. One disadvantage of this test method is that additional instrumentation is required. However, this complication is more than offset by the fact that the J-R curve can be obtained from a

single specimen. Determining a J-R curve with the basic method requires tests on multiple specimens. The most common single-specimen test technique is the unloading compliance method, which is illustrated in Figure 7.25. The crack length is computed at regular intervals during the test by partially unloading the specimen and measuring the compliance. As the crack grows, the specimen becomes more compliant (less stiff). The various J testing standards provide polynomial expressions that relate a/W to compliance. Table A7.3 in Appendix 7 lists these compliance equations for bend and compact specimens.

CTOD TESTING

The first CTOD test standard was published in Great Britain in 1979 [19]. Several years later, ASTM published E 1290, an American version of the CTOD standard. ASTM E 1290 has been revised several times, and the most recent version (as of this writing) was published in 2002 [20]. The original British CTOD test standard has been superseded by BS 7448 [10], which combines K, J, and CTOD testing into a single standard. ASTM E 1820 [4] also combined these three cracktip parameters into a single testing standard, but E 1290 is still maintained by the ASTM Committee E08 on Fatigue and Fracture. The CTOD test methods in E 1290 and E 1820 are similar, but the latter standard includes provisions for generating a CTOD resistance curve. The discussion in this section focuses primarily on the ASTM E 1820 test method. ASTM E 1820 includes both a basic and resistance curve procedure for CTOD, much like the J test methodology in this standard. The test method in E 1290 is comparable to the basic procedure. The basic procedure, where stable crack growth is not considered in the analysis, is described next. This is followed by a description of the CTOD resistance curve procedure.

UNIT V - FAILURE ANALYSIS TOOLS

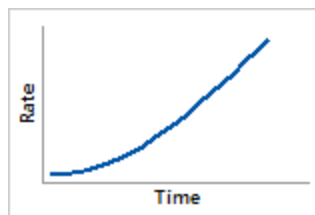
Hazard functions in reliability analysis

The hazard function is the instantaneous rate of failure at a given time. Characteristics of a hazard function are frequently associated with certain products and applications. Different hazard functions are modeled with different distribution models. You can also model hazard functions nonparametrically.

Increasing hazard function

Indicates that items are more likely to fail with time. For example, many mechanical items that are prone to stress or fatigue have an increased risk of failure over the lifetime of the product. Engineers might use a test to simulate wear-out stress. For example, engineers could simulate extended usage of a light bulb over time and then record the time until a failure occurs.

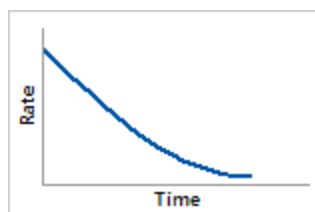
A Weibull distribution is often used to model this type of wear-out failure.



Decreasing hazard function

Indicates failures that are more likely to occur early in the life of a product. One example is products or parts composed of metals that harden with use and thus grow stronger as time passes. Or errors in a computer program, which are more likely near the release of a new software program, but then decrease as time passes.

Often, this type of data can be modeled using a Weibull distribution with a shape parameter less than 1.



Constant hazard function

Indicates failures that are equally likely to occur at any time in the product's life. This relatively constant period of low failure risk characterizes the middle portion of the Bathtub Curve.

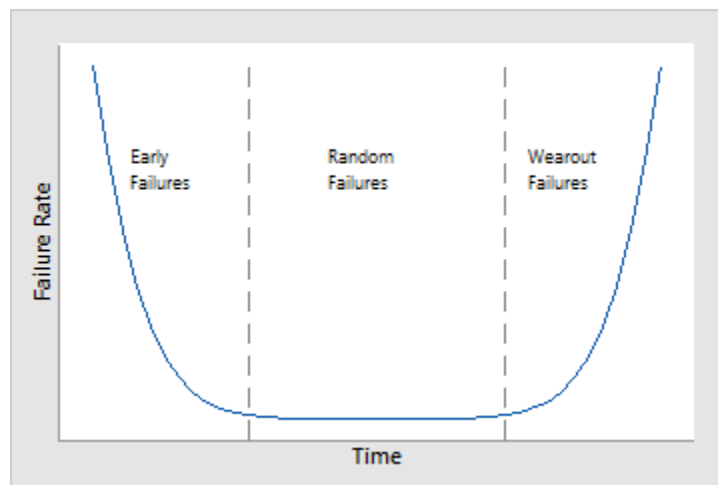
This function can be modeled using the exponential distribution.



Bathtub-shaped hazard function

Many products have failure rates that follow the "bathtub" curve. Often, the hazard rate is high initially, low in the center, then high again at the end of the life. Thus, the resulting curve of the three failure periods frequently resembles the shape of a bathtub. Televisions and handheld calculators are two products that commonly exhibit a bathtub-shaped hazard function. Also microprocessors, which may fail soon after being put into a computer system.

With Minitab, you can model a specific period of time in the bathtub function. Minitab models a decreasing hazard, constant hazard, or increasing hazard, but not all three sequentially over the life of the product.



What is the Poisson Distribution?

The Poisson Distribution is a tool used in probability theory statistics to predict the amount of variation from a known average rate of occurrence, within a given time frame. In other words, if the average rate at which a specific event happens within a specified time frame is known or can be

determined (e.g., Event “A” happens, on average, “x” times per hour), then the Poisson Distribution can be used as follows:

To determine how much variation there will likely be from that average number of occurrences

To determine the probable maximum and minimum number of times the event will occur within the specified time frame

Poisson Distribution theme

Companies can utilize the Poisson Distribution to examine how they may be able to take steps to improve their operational efficiency. For instance, an analysis done with the Poisson Distribution might reveal how a company can arrange staffing in order to be able to better handle peak periods for customer service calls.

The History of the Poisson Distribution

Like many statistical tools and probability metrics, the Poisson Distribution was originally applied to the world of gambling. In 1830, French mathematician Siméon Denis Poisson developed the distribution to indicate the low to high spread of the probable number of times that a gambler would win at a gambling game – such as baccarat – within a large number of times that the game was played. (Unfortunately, the gambler paid no heed to Poisson’s prediction of the probabilities of his obtaining only a certain number of wins, and lost heavily.) The wide range of possible applications of Poisson’s statistical tool became evident several years later, during World War II, when a British statistician used it to analyze bomb hits in the city of London. R.D. Clarke refined the Poisson Distribution as a statistical model and worked to reassure the British government that the German bombs fell randomly, or purely by chance, and that its enemies lacked sufficient information to be targeting certain areas of the city. Since then, the Poisson Distribution’s been applied across a wide range of fields of study, including medicine, astronomy, business, and sports.

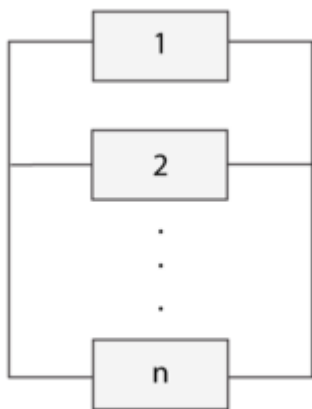
When the Poisson Distribution is Valid

The Poisson Distribution is only a valid probability analysis tool under certain conditions. It is a valid statistical model if all the following conditions exist:

- k is the number of times an event happens within a specified time period, and the possible values for k are simple numbers such as 0, 1, 2, 3, 4, 5, etc.
- No occurrence of the event being analyzed affects the probability of the event re-occurring (events occur independently).

- The event in question cannot occur twice at exactly the same time. There must be some interval of time – even if just half a second – that separates occurrences of the event.
- The probability of an event happening within a portion of the total time frame being examined is proportional to the length of that smaller portion of the time frame.
- The number of trials (chances for the event to occur) is sufficiently greater than the number of times the event does actually occur (in other words, the Poisson Distribution is only designed to be applied to events that occur relatively rarely).
- Given the above conditions, then k is a random variable, and the distribution of k is a Poisson Distribution.

Simple Parallel Systems



In a simple parallel system, as shown in the figure on the right, at least one of the units must succeed for the system to succeed. Units in parallel are also referred to as redundant units. Redundancy is a very important aspect of system design and reliability in that adding redundancy is one of several methods of improving system reliability. It is widely used in the aerospace industry and generally used in mission critical systems. Other example applications include the RAID computer hard drive systems, brake systems and support cables in bridges.

The probability of failure, or unreliability, for a system with n statistically independent parallel components is the probability that unit 1 fails and unit 2 fails and all of the other units in the system fail. So in a parallel system, all n units must fail for the system to fail. Put another way, if unit 1

succeeds or unit 2 succeeds or any of the n units succeeds, then the system succeeds. The unreliability of the system is then given by:

$$Q_s = P(X_1 \cap X_2 \cap \dots \cap X_n) = P(X_1)P(X_2|X_1)P(X_3|X_1X_2)\dots P(X_n|X_1X_2\dots X_{n-1})$$

where:

- Q_s is the unreliability of the system
- X_i is the event of failure of unit i
- $P(X_i)$ is the probability of failure of unit i

In the case where the failure of a component affects the failure rates of other components, then the conditional probabilities in equation above must be considered. However, in the case of independent components, the equation above becomes:

$$Q_s = P(X_1)P(X_2)\dots P(X_n)$$

or:

$$Q_s = \prod_{i=1}^n P(X_i)$$

Or, in terms of component unreliability:

$$Q_s = \prod_{i=1}^n Q_i$$

Observe the contrast with the series system, in which the system reliability was the product of the component reliabilities; whereas the parallel system has the overall system unreliability as the product of the component unreliabilities.

The reliability of the parallel system is then given by:

$$R_s = 1 - Q_s = 1 - (Q_1 \cdot Q_2 \cdot \dots \cdot Q_n) = 1 - [(1 - R_1) \cdot (1 - R_2) \cdot \dots \cdot (1 - R_n)] = \prod_{i=1}^n (1 - R_i)$$

Example: Calculating the Reliability with Components in Parallel

Consider a system consisting of three subsystems arranged reliability-wise in parallel. Subsystem 1 has a reliability of 99.5%, Subsystem 2 has a reliability of 98.7% and Subsystem 3 has a reliability of 97.3% for a mission of 100 hours. What is the overall reliability of the system for a 100-hour mission?

Since the reliabilities of the subsystems are specified for 100 hours, the reliability of the system for a 100-hour mission is:

$$R_s = 1 - (1 - 0.9950) \cdot (1 - 0.9870) \cdot (1 - 0.9730) = 1 - 0.0000017550 = 0.999998245$$

Effect of Component Reliability in a Parallel Configuration

When we examined a system of components in series, we found that the least reliable component has the biggest effect on the reliability of the system. However, the component with the highest reliability in a parallel configuration has the biggest effect on the system's reliability, since the most reliable component is the one that will most likely fail last. This is a very important property of the parallel configuration, specifically in the design and improvement of systems.

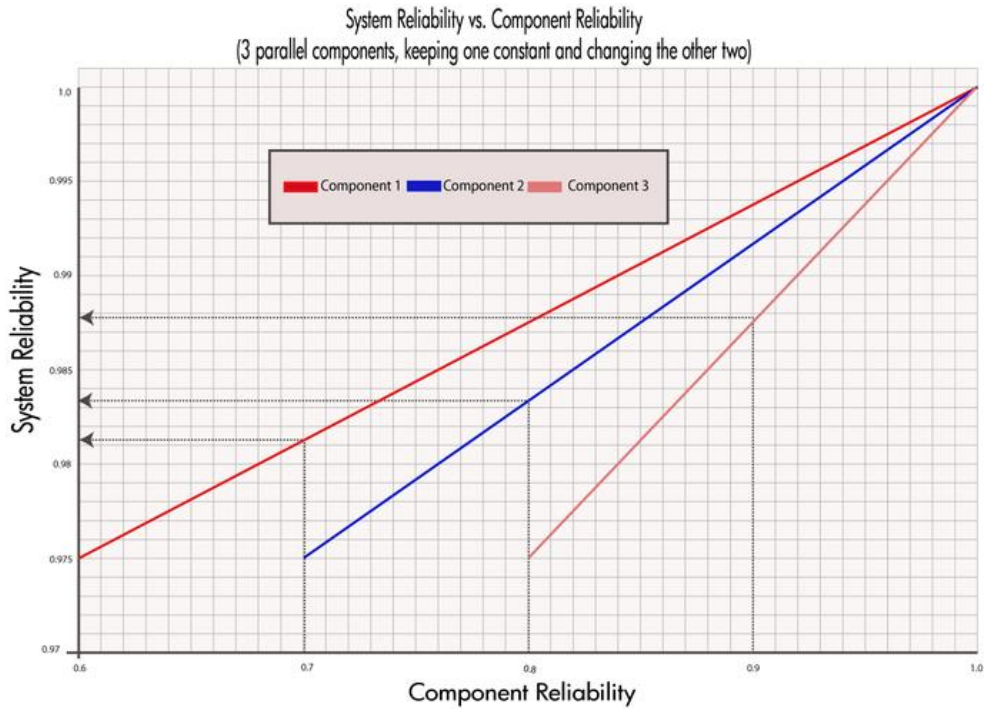
Example: Effect of a Component's Reliability in a Parallel System

Consider three components arranged reliability-wise in parallel with $R_1 = 60$, $R_2 = 70$ and $R_3 = 80$ (for a given time). The corresponding reliability for the system is $R_s = 97.6$. In the following table, we can examine the effect of each component's reliability on the overall system reliability. The first row of the table shows the given reliability for each component and the corresponding system reliability for these values. In the second row, the reliability of Component 1 is increased by a value of 10% while keeping the reliabilities of the other two components constant. Similarly, by increasing the reliabilities of Components 2 and 3 in the third and fourth rows by a value of 10% while keeping the reliabilities of the other components at the given values, we can observe the effect of each component's reliability on the overall system reliability. It is clear that the highest value for the system's reliability was achieved when the reliability of Component 3, which is the most reliable component, was increased. Once again, this is the opposite of what was encountered with a pure series system.

Table 3: System Reliability for Combinations of Components' Reliability

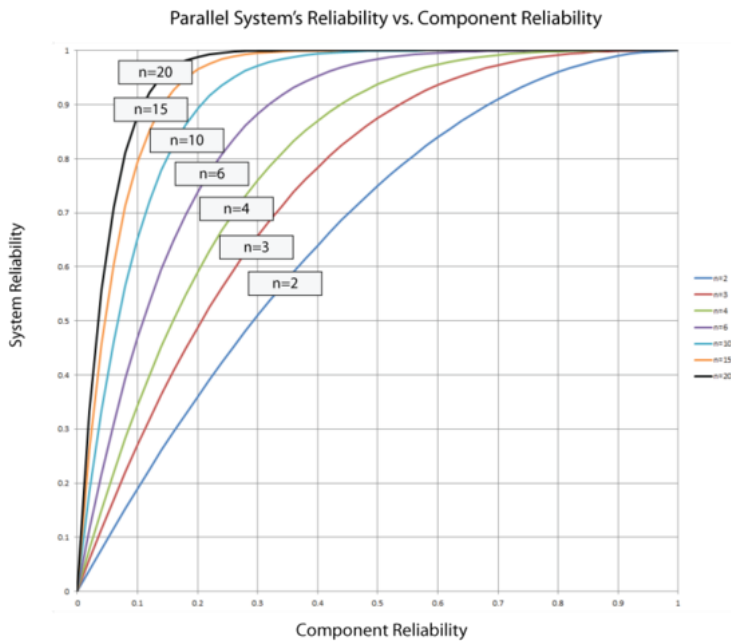
Component 1	Component 2	Component 3	System Reliability
0.6	0.7	0.8	0.976
0.7	0.7	0.8	0.982
0.6	0.8	0.8	0.984
0.6	0.7	0.9	0.988

This conclusion can also be illustrated graphically, as shown in the following plot.



Effect of Number of Components in a Parallel System

In the case of the parallel configuration, the number of components has the opposite effect of the one observed for the series configuration. For a parallel configuration, as the number of components/subsystems increases, the system's reliability increases.



The following plot illustrates that a high system reliability can be achieved with low-reliability

components, provided that there are a sufficient number of components in parallel. Note that this plot is the mirror image of the one above that presents the effect of the number of components in a series configuration.

Example: Effect of the Number of Components in a Parallel System

Consider a system that consists of a single component. The reliability of the component is 60%, thus the reliability of the system is 60%. What would the reliability of the system be if the system were composed of two, four or six such components in parallel?

Table 4: System reliability as a function of the number of components.

Number of components	System Reliability
1	0.6
2	0.84
4	0.9744
6	0.9959

Clearly, the reliability of a system can be improved by adding redundancy. However, it must be noted that doing so is usually costly in terms of additional components, additional weight, volume, etc.

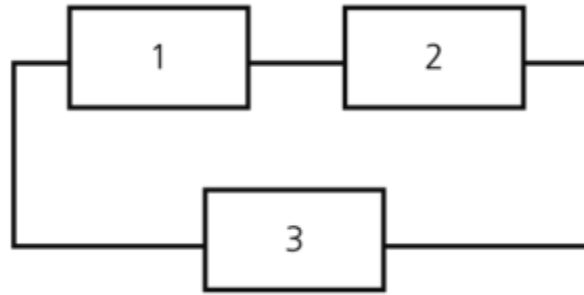
Reliability optimization and costs are covered in detail in [Component Reliability Importance](#).

Combination of Series and Parallel

While many smaller systems can be accurately represented by either a simple series or parallel configuration, there may be larger systems that involve both series and parallel configurations in the overall system. Such systems can be analyzed by calculating the reliabilities for the individual series and parallel sections and then combining them in the appropriate manner. Such a methodology is illustrated in the following example.

Example: Calculating the Reliability for a Combination of Series and Parallel

Consider a system with three components. Units 1 and 2 are connected in series and Unit 3 is connected in parallel with the first two, as shown in the next figure.



FAILURE MODE AND EFFECTS ANALYSIS (FMEA)

Quality Glossary Definition: Failure mode effects analysis (FMEA)

Also called: potential failure modes and effects analysis; failure modes, effects and criticality analysis (FMECA)

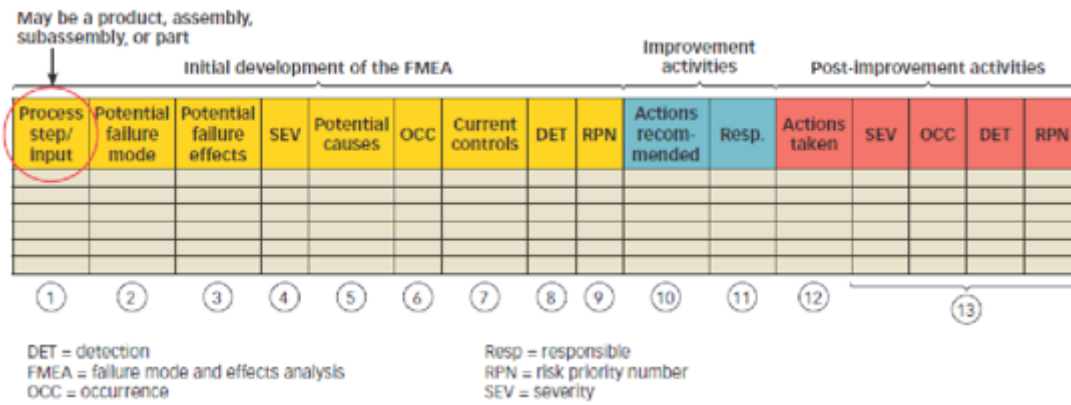
Begun in the 1940s by the U.S. military, failure modes and effects analysis (FMEA) is a step-by-step approach for identifying all possible failures in a design, a manufacturing or assembly process, or a product or service. It is a common process analysis tool.

- **"Failure modes"** means the ways, or modes, in which something might fail. Failures are any errors or defects, especially ones that affect the customer, and can be potential or actual.
- **"Effects analysis"** refers to studying the consequences of those failures.

Failures are prioritized according to how serious their consequences are, how frequently they occur, and how easily they can be detected. The purpose of the FMEA is to take actions to eliminate or reduce failures, starting with the highest-priority ones.

Failure modes and effects analysis also documents current knowledge and actions about the risks of failures, for use in continuous improvement. FMEA is used during design to prevent failures. Later it's used for control, before and during ongoing operation of the process. Ideally, FMEA begins during the earliest conceptual stages of design and continues throughout the life of the product or service.

- When to use FMEA
- FMEA procedure
- FMEA example
- FMEA resources



Failure Modes and Effects Analysis Example

WHEN TO USE FMEA

- When a process, product, or service is being designed or redesigned, after quality function deployment (QFD)
- When an existing process, product, or service is being applied in a new way
- Before developing control plans for a new or modified process
- When improvement goals are planned for an existing process, product, or service
- When analyzing failures of an existing process, product, or service
- Periodically throughout the life of the process, product, or service

FMEA PROCEDURE

Note: This is a general procedure. Specific details may vary with standards of your organization or industry. Before undertaking an FMEA process, learn more about standards and specific methods in your organization and industry through other references and training.

1. Assemble a cross-functional team of people with diverse knowledge about the process, product or service, and customer needs. Functions often included are: design, manufacturing, quality, testing, reliability, maintenance, purchasing (and suppliers), sales, marketing (and customers), and customer service.
2. Identify the scope of the FMEA. Is it for concept, system, design, process, or service? What are the boundaries? How detailed should we be? Use flowcharts to identify the scope and to make sure every team member understands it in detail.
3. Fill in the identifying information at the top of your FMEA form. (Figure 1 shows a typical format.) The remaining steps ask for information that will go into the columns of the form.

Failure	Failure Mode	Potential Effects of Failure	O	Potential Causes of Failure	O	Current Process Controls	P	D	S	RPN	Recommended Action(s)	Residual Risk (RPN)	Action Plan				
													When Done	By Whom	Cost		
Depressure of oil level reported by customer	Does not stop operation	Customer may experience discomfort if oil level drops below 10% remaining	5	Oil level low	5	Oil level sensor not working	5	500	50								
				Oil level sensor not working	3	Oil level sensor not working	10	100	30								
				Oil level sensor not working	2	Oil level sensor not working	10	100	10								
Engine oil level reported by customer	Does not stop operation	Customer may experience discomfort if oil level drops below 10% remaining	5	Oil level low	2	Oil level sensor not working	2	100	10								
				Oil level sensor not working	2	Oil level sensor not working	1	100	10								
Engine oil level reported by customer	Does not stop operation	Customer may experience discomfort if oil level drops below 10% remaining	5	Oil level low	1	Oil level sensor not working	1	100	10								
				Oil level sensor not working	2	Oil level sensor not working	10	100	10								

Figure 1: FMEA Example

- Identify the functions of your scope. Ask, "What is the purpose of this system, design, process, or service? What do our customers expect it to do?" Name it with a verb followed by a noun. Usually one will break the scope into separate subsystems, items, parts, assemblies, or process steps and identify the function of each.
- For each function, identify all the ways failure could happen. These are potential failure modes. If necessary, go back and rewrite the function with more detail to be sure the failure modes show a loss of that function.
- For each failure mode, identify all the consequences on the system, related systems, process, related processes, product, service, customer, or regulations. These are potential effects of failure. Ask, "What does the customer experience because of this failure? What happens when this failure occurs?"
- Determine how serious each effect is. This is the severity rating, or S. Severity is usually rated on a scale from 1 to 10, where 1 is insignificant and 10 is catastrophic. If a failure mode has more than one effect, write on the FMEA table only the highest severity rating for that failure mode.
- For each failure mode, determine all the potential root causes. Use tools classified as cause analysis tools, as well as the best knowledge and experience of the team. List all possible causes for each failure mode on the FMEA form.
- For each cause, determine the occurrence rating, or O. This rating estimates the probability of failure occurring for that reason during the lifetime of your scope. Occurrence is usually rated on a scale from 1 to 10, where 1 is extremely unlikely and 10 is inevitable. On the FMEA table, list the occurrence rating for each cause.
- For each cause, identify current process controls. These are tests, procedures or mechanisms that you now have in place to keep failures from reaching the customer. These controls might

prevent the cause from happening, reduce the likelihood that it will happen or detect failure *after* the cause has already happened but *before* the customer is affected.

11. For each control, determine the detection rating, or D. This rating estimates how well the controls can detect either the cause or its failure mode after they have happened but before the customer is affected. Detection is usually rated on a scale from 1 to 10, where 1 means the control is absolutely certain to detect the problem and 10 means the control is certain not to detect the problem (or no control exists). On the FMEA table, list the detection rating for each cause.
12. *Optional for most industries:* Ask, "Is this failure mode associated with a critical characteristic?" (Critical characteristics are measurements or indicators that reflect safety or compliance with government regulations and need special controls.) If so, a column labeled "Classification" receives a Y or N to show whether special controls are needed. Usually, critical characteristics have a severity of 9 or 10 and occurrence and detection ratings above 3.
13. Calculate the risk priority number, or RPN, which equals $S \times O \times D$. Also calculate Criticality by multiplying severity by occurrence, $S \times O$. These numbers provide guidance for ranking potential failures in the order they should be addressed.
14. Identify recommended actions. These actions may be design or process changes to lower severity or occurrence. They may be additional controls to improve detection. Also note who is responsible for the actions and target completion dates.
15. As actions are completed, note results and the date on the FMEA form. Also, note new S, O, or D ratings and new RPNs.

FMEA EXAMPLE

A bank performed a process FMEA on their ATM system. Figure 1 shows part of it: the function "dispense cash" and a few of the failure modes for that function. The optional "Classification" column was not used. Only the headings are shown for the rightmost (action) columns.

Notice that RPN and criticality prioritize causes differently. According to the RPN, "machine jams" and "heavy computer network traffic" are the first and second highest risks.

One high value for severity or occurrence times a detection rating of 10 generates a high RPN. Criticality does not include the detection rating, so it rates highest the only cause with medium to high values for both severity and occurrence: "out of cash." The team should use their experience and judgment to determine appropriate priorities for action.